

**Enhanced rock-slope failure following ice-sheet deglaciation: timing and causes**

Journal:	<i>Earth Surface Processes and Landforms</i>
Manuscript ID:	ESP-13-0185.R2
Wiley - Manuscript type:	Paper
Date Submitted by the Author:	n/a
Complete List of Authors:	Ballantyne, Colin; University of St Andrews, School of Geography and Geosciences Wilson, Peter; University of Ulster, School of Environmental Sciences Gheorghiu, Delia; SUERC, NERC Cosmogenic Isotope Analysis Facility Rodés, Àngel; SUERC, NERC Cosmogenic Isotope Analysis Facility
Keywords:	paraglacial, rock-slope failure, surface exposure dating, stress release, palaeoseismicity

SCHOLARONE™  
Manuscripts

Review

## Enhanced rock-slope failure following ice-sheet deglaciation: timing and causes

Colin K. Ballantyne<sup>1\*</sup>, Peter Wilson<sup>2</sup>, Delia Gheorghiu<sup>3</sup> and Àngel Rodés<sup>3</sup>

<sup>1</sup> School of Geography and Geosciences, University of St Andrews, Scotland, UK.

<sup>2</sup> School of Environmental Sciences, University of Ulster, Coleraine, UK.

<sup>3</sup> NERC Cosmogenic Isotope Analysis Facility, SUERC, East Kilbride, G75 0QF, UK

• Correspondence to Colin K. Ballantyne, School of Geography and Geosciences, University of St Andrews, Fife KY16 9AL, Scotland, UK. Email: [ckb@st-andrews.ac.uk](mailto:ckb@st-andrews.ac.uk)

**ABSTRACT:** The temporal pattern of rock-slope failures (RSFs) following Late Pleistocene deglaciation on tectonically stable terrains is controversial: previous studies variously suggest (1) rapid response due to removal of supporting ice ('debuttressing'), (2) a progressive decline in RSF frequency, (3) a millennial-scale delay before peak RSF activity. We test these competing models through <sup>10</sup>Be exposure dating of five closely-spaced quartzite RSFs on the Isle of Jura, Scotland, to establish the relationship between timing of failure and those of deglaciation, episodes of rapid warming and periods of rapid glacio-isostatic uplift. All five dated RSFs occurred at least 720–2240 years after deglaciation, with the probability of failure peaking ~2 ka after deglaciation, consistent with millennial-scale delay model (3). This excludes debuttressing as an immediate cause of failure, though it is likely that time-dependent stress release due to deglacial unloading resulted in progressive development of failure planes within the rock. Thaw of permafrost ice in joints is unlikely to have been a prime trigger of failure as some RSFs occurred several centuries after the onset of interstadial warming. Conversely, the timespan of the RSFs coincides with the period of maximum glacio-isostatic crustal uplift, suggesting that failure was triggered by uplift-driven seismic events acting on fractured rock masses. Implications of this and related research are: (1) that retreat of the last Pleistocene ice sheets across tectonically-stable mountainous terrains was succeeded by a period of enhanced rock-slope failure due to deglacial unloading and probably uplift-driven seismicity; (2) that the great majority of RSFs in the British Isles outside the limits of Loch Lomond Stadial (= Younger Dryas) glaciation are of Lateglacial (pre-Holocene) age; and (3) numerous RSFs must also have occurred inside Loch Lomond Stadial glacial limits, but that runout debris was removed by LLS glaciers.

**Keywords:** Rock-slope failure; paraglacial; surface exposure dating; stress release; palaeoseismicity.

## Introduction

Many formerly-glaciated mountains are characterized by numerous large-scale postglacial rock-slope failures (RSFs) in the form of major rockfalls, topples, rockslides, rock avalanches or deep-seated gravitational slope deformations. Such RSFs are often described as *paraglacial*, implying that failure has been conditioned by the preceding episode of glaciation and deglaciation, though the role of deglacial stress release and its interaction with other factors (such as progressive failure, thaw of ice in rock joints and seismic activity) remains incompletely understood (Ballantyne, 2002; Leith *et al.*, 2011; McColl, 2012). A particularly interesting question concerns the response time of major postglacial RSFs following deglaciation, and its implications for the factors responsible for triggering failure: do potentially unstable rockwalls respond rapidly to ice-sheet thinning and associated changes in stress, or are failure events distributed throughout postglacial time?

Surface exposure dating using cosmogenic isotopes (principally  $^{10}\text{Be}$  and  $^{36}\text{Cl}$ ) is now routinely employed to establish the age of postglacial RSFs, particularly in tectonically-active mountain belts (Ivy-Ochs and Schaller, 2010). Exposure dating of RSFs has been employed, for example, to investigate the evolution of slope deformations (Bigot-Cormier *et al.*, 2005; Agliardi *et al.*, 2009; El Bedoui *et al.*, 2009; Hippolyte *et al.*, 2009), to constrain the extent of Pleistocene glacier advances (Sanhueza-Pino *et al.*, 2011), to determine the level of hazard at former landslide sites (Welkner *et al.*, 2010), to estimate long-term rates of pre-failure sliding (Hermanns *et al.*, 2012) and to determine the contribution of RSFs to postglacial denudation and landscape evolution (Barnard *et al.*, 2001; Antinao and Gosse, 2009; Seong *et al.*, 2009; Hewitt *et al.*, 2011; Shroder *et al.*, 2011). The timing of individual dated RSFs has been variously related to deglacial unloading and stress release (Cossart *et al.*, 2008; Shroder *et al.*,

1  
2  
3 66 2011), seismic triggering or neotectonic activity (Mitchell *et al.*, 2007; Antinao and  
4  
5 67 Gosse, 2009; Sanchez *et al.*, 2010; Stock and Uhrhammer, 2010; Hermanns and  
6  
7 68 Niedermann, 2011; Hewitt *et al.*, 2011; Penna *et al.*, 2011) or climatic controls  
8  
9  
10 69 (Hermanns and Schellenberger, 2008; Hormes *et al.*, 2008; Dortch *et al.*, 2009; Ivy-  
11  
12 70 Ochs *et al.*, 2009).

13  
14 71  
15 72 Few of the above studies, however, specifically address the question of the temporal  
16  
17 73 pattern of RSFs following Late Pleistocene deglaciation and the implications of this  
18  
19 74 pattern for failure mechanisms. Cruden and Hu (1993) proposed that the frequency of  
20  
21 75 failure declines exponentially with time elapsed since deglaciation, and several  
22  
23 76 authors have suggested that the frequency of large RSFs peaks immediately after  
24  
25 77 deglaciation and declines thereafter (Abele, 1974; Soldati *et al.*, 2004). Documented  
26  
27 78 cases of rock-slope failure following recent glacier retreat (e.g. Evans and Clague,  
28  
29 79 1994; Ballantyne, 2002; Arsenault and Meigs, 2005; Allen *et al.* 2010) provide some  
30  
31 80 support for this idea. Equally, however, many of the references cited above provide  
32  
33 81 evidence of large-scale RSFs that occurred several millennia after Late Pleistocene  
34  
35 82 deglaciation (see also Hewitt *et al.*, 2008, and references therein). A global dataset of  
36  
37 83 32 dated postglacial RSFs compiled by McColl (2012) showed clustering in the early  
38  
39 84 Holocene (10–8 ka), but as these occurred in areas of variable relief, tectonic activity  
40  
41 85 and deglacial chronology, it is difficult to draw meaningful conclusions.

42  
43  
44  
45  
46 86  
47 87 Support for the idea of fairly rapid (Lateglacial and early Holocene) RSF response to  
48  
49 88 Late Pleistocene deglaciation is provided by Fauqué *et al.* (2009), who dated very  
50  
51 89 large postglacial rock avalanches in the southern Andes. Apart from one anomalously  
52  
53 90 old age, their 11 dates all fall within the period from ~13.9 ka to ~8.2 ka, with no  
54  
55 91 evidence for later activity. Similarly, using stratigraphic estimation of the approximate  
56  
57  
58  
59  
60

1  
2  
3 92 ages of rock avalanches terminating in fjords in western Norway, Longva *et al.* (2009)  
4  
5 93 concluded that 89% of the total volume of rock avalanche runout occurred during  
6  
7 94 deglaciation (~14.7 ka to ~11.7 ka), though RSF frequency apparently peaked in the  
8  
9 95 early Holocene (~11.7 ka to ~10.0 ka). Some researchers have championed the view  
10  
11 96 that a period of greatly enhanced RSF activity occurred over several millennia  
12  
13 97 following ice-sheet deglaciation as a consequence of large-magnitude seismic events  
14  
15 98 due to fault movements driven by rapid glacio-isostatic crustal uplift (e.g. Mörner,  
16  
17 99 1991, 2004; Lagerbäck, 1992; Mercier *et al.*, 2013; Cossart *et al.*, 2013), but hitherto  
18  
19  
20 100 the dating evidence required to substantiate this interpretation has been inadequate.  
21  
22

23 101  
24 102 In the Scottish Highlands, Ballantyne and Stone (2013) obtained 47 surface exposure  
25  
26 103 ages ( $^{10}\text{Be}$  and  $^{36}\text{Cl}$ ) for the runout zones of 17 catastrophic RSFs. These yielded  
27  
28 104 ages from ~17.0 ka to ~1.5 ka; ten sites produced Lateglacial and early Holocene  
29  
30 105 (> 9.8 ka) ages, and the ages for the remaining seven sites are scattered throughout  
31  
32 106 the Holocene without significant clustering. By comparing each age with the  
33  
34 107 approximate timing of deglaciation at each site, they showed that the dated Scottish  
35  
36 108 RSFs fall into two groups: 'rapid response' RSFs that failed during or within a  
37  
38 109 millennium after deglaciation (seven sites) and delayed response RSFs that failed at  
39  
40 110 various times throughout the Lateglacial and Holocene. The dataset they used,  
41  
42 111 however, suffers from three weaknesses: (1) it includes both sites deglaciated prior to  
43  
44 112 ~14.5 ka as the last British-Irish Ice Sheet retreated, and sites deglaciated much later  
45  
46 113 following limited reoccupation of Highland valleys by glacier ice during the Loch  
47  
48 114 Lomond (= Younger Dryas) Stade (LLS) of ~12.9–11.7 ka; (2) the deglaciation ages of  
49  
50 115 some sites are not accurately determined, making assessment of time elapsed since  
51  
52 116 deglaciation imprecise; and (3) the dated RSFs occur on a wide range of lithologies,  
53  
54  
55 117 so possible structural controls are ignored. The aim of the research reported here is to  
56  
57  
58  
59  
60

1  
2  
3 118 establish both the deglaciation age and timing of RSFs for a closely-spaced cluster of  
4  
5 119 RSFs on the Paps of Jura in the Inner Hebrides off the west coast of Scotland, and to  
6  
7 120 determine the temporal pattern of RSF occurrence and its implications in terms of  
8  
9 121 possible causes. This area was chosen because all RSF sites are seated on a uniform  
10  
11 122 lithology, there is no evidence for reoccupation of RSF sites by glacier ice following  
12  
13 123 ice-sheet deglaciation, and the RSFs are so closely spaced that we can assume  
14  
15 124 quasi-synchronous deglaciation, constrained by exposure ages obtained on a nearby  
16  
17 125 moraine.

### 126 127 **The Paps of Jura**

128  
129 The Paps of Jura (55°52'–55°54'N, 05°57'–06°01'W; Figure 1) comprise three  
130  
131 mountains, Beinn a'Chaolais (733 m), Beinn an Oir (785 m) and Beinn Shiantaidh  
132  
133 (757 m). All are underlain by massive fine- to medium-grained Dalradian quartzites  
134  
135 that dip ESE at 25-40° and are locally intruded by doleritic dykes (Walker, 1961;  
136  
137 Anderton, 1976, 1977, 1985).

138  
139 When the last British-Irish Ice Sheet reached its maximum extent at ~27–26 ka,  
140  
141 westwards-moving ice crossed Jura and extended to the Atlantic shelf edge, 195 km  
142  
143 west of the island (Hubbard *et al.*, 2009; Clark *et al.*, 2012). The westward reach of the  
144  
145 last ice sheet implies that it must have buried all mountain summits on Jura (cf. Fabel  
146  
147 *et al.*, 2012). This is confirmed by observations of ice-moulded bedrock at up to 660 m  
148  
149 altitude on Beinn an Oir, and by the presence of rhyolitic erratics and glacially-rounded  
150  
151 and faceted boulders on the summit (785 m) of the same mountain (Ballantyne,  
152  
153 1999), though slopes bordering the summit plateaux of all three mountains are  
154  
155 mantled by steep bouldery scree deposits. The timing of ice-sheet deglaciation is  
156  
157 poorly constrained, but a radiocarbon age obtained for a mollusc from an offshore  
158  
159  
160

1  
2  
3 145 core recovered 4 km south of Jura implies ice-sheet deglaciation of the area before  
4  
5 146 ~15 cal <sup>14</sup>C ka (Peacock, 2008; Clark *et al.*, 2012). There is no convincing evidence  
6  
7 147 for reoccupation of Jura by glacier ice during the Loch Lomond Stade of ~12.9–11.7  
8  
9 148 ka, implying that the Paps of Jura have escaped glaciation since the retreat of the last  
10  
11 149 ice sheet from the area.

12  
13  
14 150 Jura occupies a tectonically-stable intraplate location characterised by low-magnitude  
15 151 ( $M_L < 4.0$ ) seismic activity (Musson, 2007). No seismic events exceeding  $M_L$  3.5 have  
16  
17 152 been recorded on Jura or the adjacent shelf within the past ~40 years of instrumental  
18  
19 153 observations (Julian Bukits, personal communication, March 2013).  
20  
21 154

### 22 155 **The Jura RSFs**

23  
24 156

25  
26  
27 157 Ballantyne (1999) described evidence for rock-slope failure on all three mountains in  
28 158 the form of displaced rock masses and fissures on summit rims. Evidence for debris  
29  
30 159 runout associated with catastrophic failure is limited to six sites, five of which were  
31  
32 160 sampled for exposure dating and are described below. At all these sites the  
33  
34 161 morphological evidence (Figure 2) appears consistent with a single major failure  
35  
36 162 episode, though we cannot exclude the possibility at some sites of later emplacement  
37  
38 163 of debris by rockfall, debris flow or minor secondary RSF events. All RSF runout  
39  
40 164 deposits terminate abruptly at the slope foot (Figure 2), demonstrating that they have  
41  
42 165 not been modified by glacier ice and must have occurred after retreat of the last ice  
43  
44 166 sheet.  
45  
46 167

### 47 168 *Beinn Shiantaidh RSF*

48 169

49  
50 170 The Beinn Shiantaidh (BS) RSF represents a major rockslide or rock avalanche from  
51  
52 171 the eastern flank of Beinn Shiantaidh. The crown of the failure zone is represented by  
53  
54 172 an indented line of cliffs at 600-700 m altitude just below the summit (Figure 2a), and  
55  
56  
57  
58  
59  
60

1  
2  
3 173 the runout zone by a spectacular deposit of boulders that extends 380 m along the  
4  
5 174 foot of the slope and 180 m outwards over the adjacent level ground. The most  
6  
7 175 conspicuous feature of the runout zone is a massive arcuate distal ridge (Figure 2b)  
8  
9 176 that terminates abruptly outwards and encloses a depression up to 6 m deep and an  
10  
11 177 inner zone of large boulders. Dawson (1977) calculated that the deposit has a  
12  
13 178 minimum volume of 185,000 m<sup>3</sup>, implying failure of at least 0.37 Mt of rock. The BS  
14  
15 179 RSF runout deposit was interpreted by Dawson (1977) as a relict rock glacier, but this  
16  
17 180 interpretation appears unwarranted as its morphology is consistent with RSF runout  
18  
19 181 without the need to invoke internal deformation of a former body of ice or ice-rich  
20  
21 182 permafrost (Jarman *et al.*, 2013). The distal ridge is interpreted as representing impact  
22  
23 183 of avalanching debris on the level ground at the foot of the slope, which caused the  
24  
25 184 debris to accumulate as a crescentic ridge around the impact zone. Similar instances  
26  
27 185 of arcuate impact ridges developed at a basal break of slope have been documented  
28  
29 186 in NW Scotland (Ballantyne and Stone, 2009) and at the foot of quartzite mountains in  
30  
31 187 Donegal (Wilson, 2004).

32  
33  
34  
35  
36 188  
37 189 *Beinn a'Chaolais RSFs*

38  
39 190 The SE flank of Beinn a'Chaolais exhibits evidence for deep-seated gravitational slope  
40  
41 191 deformation in the form of displaced rock masses, bulging slopes and rock benches.  
42  
43 192 The Beinn a'Chaolais South (BCS) RSF apparently reflects collapse of the ridge crest  
44  
45 193 and runout of bouldery debris at the foot of a gully near the southern margin of the  
46  
47 194 displaced rock mass, forming a broad bouldery runout lobe with a gently-sloping distal  
48  
49 195 rim (Figure 2c). The Beinn a'Chaolais East (BCE) RSF runout (Figure 2d) forms a  
50  
51 196 massive debris lobe, at least 15 m thick at its distal end, near the northern margin of  
52  
53 197 the zone of displaced rock. It appears to have been sourced from near the top of the  
54  
55 198 slope where a low cliff marks the failure headscarp. The Beinn a'Chaolais West  
56  
57  
58  
59  
60



1  
2  
3 199 (BCW) failure scar is represented by a funnel-shaped re-entrant in a line of summit  
4  
5 200 cliffs. Below a broad talus cone, coarse debris extends over 200 m over gently sloping  
6  
7 201 ground in the form of two elongate lobes (Figure 2e) separated by a bedrock knoll.  
8  
9 202 Dolerite boulders on the northern lobe appear to be derived from a dyke in the summit  
10  
11 203 cliffs. Excess runout over low gradients suggests that these lobes may reflect  
12  
13 204 emplacement by RSF-generated debris flows, though they lack the pronounced  
14  
15 205 bouldery levées characteristic of rockslide-sourced debris flows on the Scottish  
16  
17 206 mainland (Ballantyne, 1992, 2007).

20  
21 207 *Beinn an Oir East RSF*  
22 208

23  
24 209 The eastern slope of Beinn an Oir also exhibits evidence for deep-seated deformation,  
25  
26 210 particularly evident in the form of a ramp of displaced bedrock. The Beinn an Oir East  
27  
28 211 (BOE) RSF is located at the southern end of this ramp, and comprises a shallow  
29  
30 212 headscarp and boulder-covered slope with limited debris runout (Figure 2f).

31  
32  
33 213 **Sampling and sample preparation**  
34 214

35  
36 215 Rock samples for  $^{10}\text{Be}$  surface exposure dating were chiseled from near-horizontal top  
37 216 surfaces of three large boulders on each of the five RSF runout zones (Figure 3). All  
38  
39 217 sampled boulder surfaces comprised apparently unweathered quartzite; weathering  
40  
41 218 rinds were absent in all cases, and boulders that could have toppled from their original  
42  
43 219 positions were avoided. Where possible, samples were obtained from boulders on the  
44  
45 220 distal part of runout zones (Figure 1) to reduce the possibility of sampling boulders  
46  
47 221 deposited by later rockfall events.  
48  
49 222

50  
51  
52 223 To establish the timing of deglaciation in the area, four additional samples were  
53 224  
54  
55 225 obtained from quartzite boulders on the Sgriob na Caillich moraine, which stretches  
56  
57 226 3.5 km WNW from the foot of Beinn an Oir and is composed of parallel belts of  
58  
59  
60

1  
2  
3 227 angular quartzite boulders, but lacks surface relief (Figures 1 and 4). Because the  
4  
5 228 moraine terminates at the Lateglacial marine limit, Dawson (1979) argued that this  
6  
7 229 feature is a medial moraine deposited during retreat and thinning of the last ice sheet,  
8  
9 230 rather than a lateral moraine marking the extent of a later glacial readvance. The large  
10  
11 231 volume of debris in the moraine and the angularity of the boulders suggests that the  
12  
13 232 moraine represents supraglacial transport of RSF debris dumped on the thinning ice  
14  
15 233 surface by failure of the rock slope SW of the summit of Beinn an Oir (now  
16  
17 234 represented by deeply-indented twin failure scars; Figure 1 and Figure 4a) then  
18  
19 235 deposited shortly afterwards as the ice downwasted. This interpretation implies that  
20  
21 236 the higher parts of the Paps of Jura above ~550 m had already emerged from the ice  
22  
23 237 surface as nunataks before the moraine was deposited, so that the age of the moraine  
24  
25 238 provides a reasonable approximation for complete deglaciation of the area. Samples  
26  
27 239 for exposure dating were taken from boulders protruding from the moraine surface to  
28  
29 240 minimise the possibility of former sediment or peat cover.  
30  
31  
32  
33

34 241 At all sites a skyline survey was carried out to allow calculation of the effects of  
35 242 topographic shielding. Multiple caliper measurements were made on each sample to  
36  
37 243 determine sample thickness, then samples were crushed and sieved. All samples  
38  
39 244 were prepared at the NERC Cosmogenic Isotope Analysis Facility at SUERC, East  
40  
41 245 Kilbride. Quartz was separated from the 250–500  $\mu\text{m}$  fraction using magnetic  
42  
43 246 separation and hexafluorosilicic acid etching. The isolated quartz was cleaned in 16%  
44  
45 247 hydrofluoric acid on a shaker table to remove remaining contaminants and meteoric  
46  
47 248  $^{10}\text{Be}$  by etching >30% of each sample, following procedures modified from Kohl and  
48  
49 249 Nishiizumi (1992). BeO targets were prepared for  $^{10}\text{Be}/^9\text{Be}$  analysis using procedures  
50  
51 250 modified from Child *et al.* (2000), and  $^{10}\text{Be}/^9\text{Be}$  ratios were measured with the 5 MV  
52  
53 251 Pelletron AMS at SUERC (Xu *et al.*, 2010).  $^{10}\text{Be}/^9\text{Be}$  ratios were normalized to NIST  
54  
55 252  
56  
57  
58  
59  
60

1  
2  
3 253 SRM 4325 with a  $^{10}\text{Be}/^9\text{Be}$  ratio of  $2.79 \times 10^{-11}$  (in agreement with Nishiizumi et al.,  
4  
5 254 2007). Secondary standard measurements scattered with less than 3% standard  
6  
7 255 deviations. The processed blank  $^{10}\text{Be}/^9\text{Be}$  ratios were between 1 and 6 % of the  
8  
9 256 sample  $^{10}\text{Be}/^9\text{Be}$  ratios and were subtracted from the measured ratios. The  
10  
11 257 uncertainty of this correction is included in the stated standard uncertainties. Details of  
12  
13  
14 258 sample locations and relevant analytical data are given in Table 1.

### 259 **Exposure age calibration and scaling**

16  
17 259  
18 260  
19  
20 261 Exposure ages were calculated using the CRONUS-Earth online calculator  
21 262 (Developmental version; wrapper script 2.2, main calculator 2.1, constants 2.2.1,  
22 263 muons 1.1; Balco et al., 2008) and calibrated using two locally-derived  $^{10}\text{Be}$  production  
23 264 rates (LPRs) to minimise scaling uncertainty (e.g. Balco et al., 2009; Kaplan et al.,  
24 265 2010; Balco, 2011). The first, the Loch Lomond local production rate (LL LPR) is  
25 266 based on  $^{10}\text{Be}$  concentration in samples from boulders on the terminal moraine of the  
26 267 glacier that advanced to the southern end of Loch Lomond, ~95 km ENE of the Paps  
27 268 of Jura, during the Loch Lomond Stade (Fabel *et al.*, 2012; D. Fabel, personal  
28 269 communication, November 2012). The age of this moraine is independently  
29 270 constrained by radiocarbon dating (MacLeod *et al.*, 2011), and the measured  $^{10}\text{Be}$   
30 271 concentrations imply a reference  $^{10}\text{Be}$  production rate (Lm scaling) of  $3.92 \pm 0.18$   
31 272 atoms  $\text{g}^{-1} \text{a}^{-1}$ .  
32  
33  
34  
35  
36  
37  
38  
39  
40  
41  
42  
43  
44  
45  
46  
47

48 274 The second LPR we employ is the NWH11.6 LPR. The calibration data can be  
49 275 accessed at [http://depts.washington.edu/cosmolab/cronus/cronus\\_cal.html](http://depts.washington.edu/cosmolab/cronus/cronus_cal.html), and  
50 276 further site and analytical details are given in Ballantyne and Stone (2012). This LPR  
51 277 is based on samples from glacially-deposited boulders and bedrock surfaces inside  
52 278 the limits of small glaciers that formed in NW Scotland (160–180 km north of the Paps  
53  
54  
55 279  
56  
57  
58  
59  
60

1  
2  
3 280 of Jura) during the Loch Lomond Stade. This LPR is based on an assigned deglacial  
4  
5 281 exposure age of  $11.6 \pm 0.3$  ka, yielding a reference  $^{10}\text{Be}$  production rate (Lm scaling)  
6  
7 282 of  $4.20 \pm 0.14$  atoms  $\text{g}^{-1} \text{a}^{-1}$  for an assumed surface erosion rate of  $1 \text{ mm ka}^{-1}$ . These  
8  
9 283 two LPRs were selected as they bracket the range of possible exposure ages for our  
10  
11 284 samples (cf. Fabel *et al.*, 2012). Use of the NWH11.6 LPR produces exposure ages  
12  
13 285 6.85–7.00% younger than use of the LL LPR, or roughly 1000 years younger for LL  
14  
15 286 LPR ages of 14–15 ka. To avoid citation of paired ages, we base the discussion below  
16  
17 287 on the ages derived using LL LPR, with the caveat that true exposure ages may be up  
18  
19 288 to 7% younger. Where citation of both ages is necessary, the age derived using LL  
20  
21 289 LPR is cited first, followed in brackets by the age derived using NWH11.6 LPR.  
22  
23  
24

25 290  
26 291 An additional advantage of using LPRs is that the variability amongst different  
27  
28 292 production rate scaling schemes (the St, Lm, Li, De and Du schemes of the CRONUS-  
29  
30 293 Earth calculator) is reduced. Here we report ages using the time-dependent Lm  
31  
32 294 scheme (Lal, 1991; Stone 2000), which is widely used in studies of deglaciation  
33  
34 295 chronology in the British Isles. Lm scaling produces the youngest ages for our  
35  
36 296 samples; other scaling schemes produce ages up to 1.5% older. We assume a  
37  
38 297 surface erosion rate ( $\varepsilon$ ) of  $1 \text{ mm ka}^{-1}$ , which is reasonable for crystalline rocks  
39  
40 298 (Ballantyne, 2010);  $\varepsilon = 0$  reduces our reported ages by  $\sim 1\%$ , and  $\varepsilon = 2 \text{ mm ka}^{-1}$   
41  
42 299 increases the reported ages by a similar margin. Assumption of a particular LPR,  
43  
44 300 scaling scheme or erosion rate has negligible effect on the temporal *pattern* of RSFs  
45  
46 301 relative to deglaciation age, as all ages are affected proportionally. Uncertainties cited  
47  
48 302 below are external (total) uncertainties at  $\pm 1\sigma$ .  
49  
50  
51  
52

53 303  
54 304  
55  
56  
57  
58  
59  
60

## Results

Table 2 and Figure 5 summarise the exposure dating results for both LPRs. Tests of difference between ages were based on the two-sample difference of means test.

### *Deglaciation ages*

Samples SNC-06 and SNC-07 from the Sgriob na Caillich medial moraine yielded almost identical ages ( $16.88 \pm 1.10$  ka and  $16.82 \pm 1.03$  ka respectively, with a weighted mean age of  $16.84 \pm 0.93$  ka). Both samples were obtained at a point where the moraine crosses a bedrock knoll. Sample SNC-02 ( $14.01 \pm 1.69$  ka) and sample SNC-03 ( $12.35 \pm 1.41$  ka) both differ significantly from this weighted mean age (at  $p < 0.1$  and  $p < 0.05$  respectively), and we interpret these ages as reflecting former burial of the boulders from which they were obtained under sediment and/or peat cover (Putkonen and Swanson, 2003; Heyman *et al.*, 2011), consistent with the absence of relief on the medial moraine (Figure 4). Both of these ages, moreover, post-date the oldest RSFs in the Paps of Jura (the Beinn Shiantaidh and Beinn a'Chaolais West RSFs; Table 2), and as the RSF runout deposits show no sign of glacial modification it is reasonable to infer complete deglaciation of Jura before the oldest RSFs occurred. The ages obtained for SNC-02 and SNC-03 also postdate rapid warming at the onset of the Lateglacial Interstade at  $\sim 14.7$  ka (Brooks and Birks, 2000; Brooks *et al.*, 2012), by which time the ice-sheet margin had retreated inland from the western seaboard of mainland Scotland (Hubbard *et al.*, 2009; Ballantyne and Stone, 2012; Clark *et al.*, 2012), implying prior deglaciation of most or all of the Inner Hebrides. We therefore exclude both these ages and assume that the weighted mean age of  $16.84 \pm 0.93$  ka ( $15.75 \pm 0.53$  ka) for samples SNC-06 and SNC-07 approximates the timing of the deglaciation of west-central Jura. This conclusion is consistent with the minimum deglaciation age of  $\sim 15$  cal  $^{14}\text{C}$  ka obtained for a mollusc

1  
2  
3 332 recovered from an offshore core recovered 4 km south of Jura (Peacock, 2008). If  
4  
5 333 sample SNC-02 ( $14.01 \pm 1.69$  ka) is included, the weighted mean age for deglaciation  
6  
7 334 differs only slightly ( $16.61 \pm 0.88$  ka), and does not significantly affect analysis of RSF  
8  
9 335 ages in terms of time elapsed since deglaciation.

11 336  
12 337 *RSF ages*

13  
14 338  $^{10}\text{Be}$  exposure ages for individual RSF samples (LL LPR) range from  $20.57 \pm 1.56$  ka  
15  
16  
17 339 to  $8.54 \pm 0.52$  ka (Figure 5 and Table 2). However, samples BS-03 ( $19.22 \pm 1.14$  ka)  
18  
19 340 and BOE-03 ( $20.57 \pm 1.56$  ka) produced ages significantly older ( $p < 0.01$ ) than the  
20  
21 341 weighted mean deglaciation age implied by the Sgriob na Caillich moraine samples.  
22  
23 342 Both ages are also significantly older ( $p < 0.001$ ) than the others obtained from the  
24  
25 343 same RSF runout deposit. We attribute these two anomalies to sampling boulders  
26  
27 344 derived from at or near the former cliff face prior to failure, and thus exposed to cosmic  
28  
29 345 radiation before failure occurred, a common occurrence in some RSF runout deposits  
30  
31 346 as boulders derived from near the pre-failure rock face may be rafted on the surface of  
32  
33 347 the mobile debris (Ivy-Ochs *et al.*, 2009; Ivy-Ochs and Schaller, 2010). These two  
34  
35 348 ages are therefore excluded from further analysis. We also exclude sample BCE-02  
36  
37 349 ( $9.56 \pm 0.57$  ka), which is significantly younger ( $p < 0.001$ ) the two other ages  
38  
39 350 ( $13.92 \pm 0.84$  ka and  $13.44 \pm 0.81$  ka) obtained from the same site, and probably  
40  
41 351 reflects later rockfall deposition after the main failure at this site.  
42  
43  
44  
45

46 352  
47 353 After exclusion of these three ages, three of the RSF runout deposits (BS, BCS and  
48  
49 354 BCE) yielded pairs or triplets of statistically indistinguishable exposure ages with  
50  
51 355 reduced chi-square values  $< 1.0$ , consistent with sampling from a single age  
52  
53 356 population (Balco, 2011). For these three runout deposits we calculated uncertainty-  
54  
55 357 weighted mean ages of  $15.11 \pm 0.81$  ka,  $14.81 \pm 0.56$  ka and  $13.67 \pm 0.73$  ka  
56  
57 358 respectively for the timing of rock-slope failure (Table 2). The remaining two runout  
58  
59  
60

1  
2  
3 359 sites yielded exposure ages that differ from all others from the same site at  $p < 0.05$ .  
4  
5 360 In these cases we infer that the main failure event is represented by the oldest post-  
6  
7 361 deglaciation age from these sites, represented by sample BCW-04 ( $15.37 \pm 0.92$  ka)  
8  
9 362 and sample BOE-05 ( $14.38 \pm 0.88$  ka), with younger ages reflecting boulder  
10  
11 363 deposition by later debris-flow events (at BCW) or rockfall (at BOE). It is also possible  
12  
13 364 that the younger ages from these two sites represent shielding by former sediment  
14  
15 365 cover (Putkonen and Swanson, 2003; Heyman *et al.*, 2011), though we encountered  
16  
17 366 no evidence for sediment or peat cover on any of the bouldery RSF deposits (Figure  
18  
19 367 3). Interpretation of the exposure ages for samples BCW-04 and BOE-05 as  
20  
21 368 representative for these RSFs implies that failure at all five dated Jura RSF sites  
22  
23 369 occurred between  $15.37 \pm 0.92$  ka ( $14.37 \pm 0.74$  ka) and  $13.67 \pm 0.73$  ka  
24  
25 370 ( $12.78 \pm 0.57$  ka). However, it is possible that one or more of the younger ages  
26  
27 371 obtained for BCW and BOE identify the timing of initial failure and that the ages  
28  
29 372 obtained for BCW-04 and BOE-05 represent nuclide inheritance, though this appears  
30  
31 373 unlikely as it implies a complex exposure history for these samples that has  
32  
33 374 fortuitously produced ages similar to those of the other three dated RSFs. Thus  
34  
35 375 although the BCW samples are interpreted below as representing rock-slope failure at  
36  
37 376  $15.37 \pm 0.92$  ka, we cannot exclude the possibility of later or possibly renewed failure,  
38  
39 377 as represented by samples BCW-01 ( $12.06 \pm 0.72$  ka) or BCW-03 ( $10.08 \pm 0.61$  ka).  
40  
41 378 Similarly, although the two post-deglaciation ages obtained for the BOE RSF are  
42  
43 379 interpreted as indicating failure at  $14.38 \pm 0.88$  ka, we cannot exclude the possibility of  
44  
45 380 later failure at  $8.54 \pm 0.52$  ka (sample BOE-04).  
46  
47  
48  
49  
50  
51 381  
52 382 In summary, the weighted mean ages obtained for three RSFs (BS, BCS and BCE)  
53  
54 383 and the oldest postglacial ages obtained for the remaining two RSFs (BCW, BOE) all  
55  
56 384 fall within the period of the Late Devensian (Late Weichselian) Lateglacial between  
57  
58  
59  
60

1  
2  
3 385 15.37 ± 0.92 ka (14.37 ± 0.75 ka) to 13.67 ± 0.73 ka (12.78 ± 0.57 ka), and thus imply  
4  
5 386 that at least three of the RSFs (and probably all five) occurred in the interval between  
6  
7 387 ice-sheet deglaciation at ~16.8 ka (~15.8 ka) and the beginning of the LLS at ~12.9  
8  
9 388 ka. However, if the younger ages obtained for BCW and BOE are representative for  
10  
11 389 these sites, these imply that failure (or renewed failure) at BCW may have occurred as  
12  
13 390 late as 10.08 ± 0.61 ka (9.43 ± 0.50 ka) and that at BOE as late as 8.54 ± 0.52 ka  
14  
15 391 (7.99 ± 0.42 ka).  
16  
17  
18

### 19 392 **RSF timing and causes of failure** 20 393

21 394  
22 395 An extensive body of literature suggests a temporal and causal association between  
23  
24 396 deglaciation of steep rockwalls and subsequent catastrophic rock-slope failure, both  
25  
26 397 with regard to recent glacier shrinkage (Evans and Clague, 1994; Ballantyne, 2002;  
27  
28 398 Arsenault and Meigs, 2005) and Late Pleistocene or early Holocene deglaciation (e.g.  
29  
30 399 Soldati *et al.*, 2004; Blikra *et al.*, 2006; Fauqué *et al.*, 2009; Longva *et al.*, 2009;  
31  
32 400 Mercier *et al.*, 2013). Explanations for this association fall into three main classes: (1)  
33  
34 401 processes associated with deglaciation or deglacial unloading at the local scale  
35  
36 402 ('debuttressing' and paraglacial stress release); (2) warming and thaw of permafrost  
37  
38 403 ice in joints; and (3) processes associated with deglacial unloading at a regional scale  
39  
40 404 (glacio-isostatic crustal uplift and associated seismicity). Two or more of these may  
41  
42 405 operate in conjunction to reduce rock-mass strength to a state of critical conditional  
43  
44 406 stability and ultimately to trigger failure. Examination of the timing of the individual  
45  
46 407 RSFs on Jura in relation to deglaciation (Figure 6) and regional environmental  
47  
48 408 changes (Figure 7) nevertheless allows some assessment of causes of failure.  
49  
50  
51  
52  
53  
54 409  
55 410  
56  
57  
58  
59  
60



1  
2  
3 411 *Deglaciation, 'debuttressing' and stress release*

4  
5 412 The exposure ages reported above (Table 2) imply that all five dated RSFs on Jura  
6  
7 413 occurred at least 770–2240 years after deglaciation (figure 6). The oldest RSF  
8  
9 414 (BCW) is significantly younger than the inferred timing of deglaciation at  $p < 0.1$ , and  
10  
11 415 all other RSF ages are significantly younger at  $p < 0.01$  or  $p < 0.001$ . If removal of  
12  
13 416 supporting glacier ice during deglaciation ('debuttressing') was the cause of failure,  
14  
15 417 then RSF ages should be indistinguishable from deglaciation age. The millennial-scale  
16  
17 418 delay in RSF activity following deglaciation (Figure 6) indicates with 95% confidence  
18  
19 419 that this was not so, and that 'debuttressing' can be excluded as a triggering  
20  
21 420 mechanism in the case of the exposure-dated Jura RSFs. However, as outlined  
22  
23 421 above, the Sgriob na Caillich moraine appears to represent the glacially-transported  
24  
25 422 runout debris from rock-slope failure SW of the summit of Beinn an Oir. If this  
26  
27 423 interpretation is correct, it implies that this failure occurred during ice-sheet thinning,  
28  
29 424 possibly as a direct response to glacial debuttressing as the adjacent glacier ice  
30  
31 425 surface thinned to ~550–600 m altitude, exposing the adjacent rock slope.

32  
33 426  
34 427 Paraglacial (glacially-conditioned) stress release has been widely invoked as a factor  
35  
36 428 in explaining RSFs in formerly glaciated mountains, but the process is incompletely  
37  
38 429 understood. Some authors have emphasised differential loading by glacier ice and  
39  
40 430 subsequent unloading during deglaciation in altering the state of stress within  
41  
42 431 rockwalls, others the effects of glacial erosion in changing the rockwall stress field,  
43  
44 432 and others still the role of glacier ice in suppressing *in situ* rock stresses resulting from  
45  
46 433 the tectonic and erosional history of the rock mass, with consequent reduction in  
47  
48 434 confining stress during deglaciation (e.g. Augustinus, 1995; Cossart *et al.*, 2008;  
49  
50 435 Amadei and Stephansson, 1997; Leith *et al.* 2010, 2011). Irrespective of the cause of  
51  
52 436 paraglacial stress release, there is agreement that it is responsible for fracture  
53  
54  
55  
56  
57  
58  
59  
60

1  
2  
3 437 propagation, and particularly for development of slope-parallel joints that form  
4  
5 438 potential failure planes (Hencher *et al.*, 2011; McColl, 2012). Although some authors  
6  
7 439 have rejected stress release as the cause of postglacial rock-slope failure at sites  
8  
9 440 where a millennial time lag separates deglaciation and failure (e.g. Mitchell *et al.*,  
10  
11 441 2007; Prager *et al.*, 2009; Hippolyte *et al.*, 2009; Stock and Uhrhammer, 2010), it  
12  
13 442 unquestionably plays a role in preconditioning slopes to failure, and probably accounts  
14  
15 443 for the high incidence of RSFs in formerly-glaciated steplands. This interpretation is  
16  
17 444 supported by Cossart *et al.* (2008), who showed that postglacial RSFs in the western  
18  
19 445 Alps occur where glacially-induced confining stresses were greatest. Moreover,  
20  
21 446 geotechnical modelling by Eberhardt *et al.* (2004) and Gugliemi and Cappa (2010)  
22  
23 447 indicates that the progressive loss of rock mass strength associated with paraglacial  
24  
25 448 stress release may extend over several millennia, preconditioning rock masses to  
26  
27 449 failure long after deglaciation, though failure itself may be precipitated by transient  
28  
29 450 triggering factors such as seismic activity. The millennial-scale delay in rock-slope  
30  
31 451 failure following deglaciation evident on Jura (Figure 6) is consistent with this view:  
32  
33 452 fracture propagation and consequent progressive failure due to time-dependent  
34  
35 453 release of strain energy in deglacially-unloaded rock masses might explain the  
36  
37 454 temporal pattern of failure even in the absence of specific triggering mechanisms  
38  
39 455 (Kemeny, 2003; Eberhardt *et al.*, 2004; Brideau *et al.*, 2009), though comparison with  
40  
41 456 environmental changes at the time of the Jura RSFs (Figure 7) suggest that two  
42  
43 457 triggering factors – thaw of ice in joints and seismotectonic activity – may have  
44  
45 458 precipitated failure of fractured rock.  
46  
47  
48  
49  
50

51  
52 459 *Warming and thaw of ice in ice-bonded rock*  
53 460

54  
55 461 Warming and thaw of permafrost ice within jointed rock masses has been shown to  
56  
57 462 reduce rock mass strength and trigger rock-slope failure (e.g. Davies *et al.*, 2001;  
58  
59  
60

1  
2  
3 463 Gruber and Haeberli, 2007; Haeberli *et al.*, 2008; Krautblatter *et al.*, 2012, 2013).  
4  
5 464 Permafrost is known to have developed in northern Britain in the wake of ice-sheet  
6  
7 465 retreat (Ballantyne and Harris, 1994). It is therefore possible that ice formed within  
8  
9 466 rock joints during this interval, increasing rock-slope stability, and that subsequent  
10  
11 467 thaw of ice-bonded joints induced failure of rock slopes previously weakened by stress  
12  
13 468 release and fracture propagation. Permafrost thaw was initiated by rapid warming at  
14  
15 469 the onset of the Lateglacial Interstade (~14.7 ka), when mean July temperatures in  
16  
17 470 Scotland increased by 6-7°C and mean January temperatures rose by up to ~25°C  
18  
19 471 over a few decades (Atkinson *et al.*, 1987; Brooks and Birks, 2000; Brooks *et al.*,  
20  
21 472 2012). If thaw of ice-bonded rock joints was responsible for triggering the Jura RSFs, it  
22  
23 473 would be expected that the timing of RSFs would cluster within a few centuries  
24  
25 474 following 14.7 ka. This is not the case. Irrespective of the LPR used in RSF age  
26  
27 475 calculation, most best-estimate ages of the Jura RSFs either predate, or post-date by  
28  
29 476 several centuries, this episode of rapid stadial-interstadial warming (Figure 7). The  
30  
31 477 wide uncertainties associated with the RSF ages do not permit exclusion of thaw of  
32  
33 478 ice-bonded rock as a trigger of kinematic release for individual RSFs, but this  
34  
35 479 mechanism cannot apply in all cases.

#### 480 481 *Glacio-isostatic rebound and palaeoseismicity*

482  
483 There is growing evidence that earthquake activity on passive margins and intraplate  
484  
485 areas was very much greater in the aftermath of Late Pleistocene deglaciation than at  
486  
487 present (Gregerson and Basham, 1989; Stewart *et al.*, 2000; Morner, 2005), reflecting  
488  
489 both crustal uplift due to glacio-isostatic rebound and release of regional tectonic  
50  
51 486 strain energy that had accumulated during the preceding period of ice-sheet glaciation  
52  
53 487 (Muir-Wood, 2000). Large magnitude 'endglacial' earthquakes triggered by glacio-  
54  
55 488 isostatic uplift have been implicated as RSF triggers in Scotland, Fennoscandia and  
56  
57  
58  
59  
60

1  
2  
3 490 Iceland (Sissons and Cornish, 1982a, 1982b; Lagerbäck, 1992; Ballantyne, 1997;  
4  
5 491 Mörner, 1991, 2004; Mörner *et al.*, 2000; Mercier *et al.*, 2013; Cossart *et al.*, 2013),  
6  
7 492 but in Scotland the evidence for a period of enhanced Lateglacial seismicity rests on  
8  
9 493 uncertain foundations. Earlier accounts inferring large, tectonically-induced postglacial  
10  
11 494 strike-slip faulting in western Scotland (Davenport *et al.*, 1989; Ringrose, 1989a;  
12  
13 495 Ringrose *et al.*, 1991) have been questioned, and it appears that postglacial faulting  
14  
15 496 may have been limited to the formation of metre-high scarps associated with  
16  
17 497 differential crustal rebound (Firth and Stewart, 2000; Stewart *et al.*, 2001). Smith *et al.*  
18  
19 498 (2009) have suggested that markedly greater (> 5 m) Lateglacial vertical movement  
20  
21 499 occurred along a listric fault on the Island of Raasay, (160 km N of the Paps of Jura)  
22  
23 500 but the evidence for this may represent, at least in part, the effects of deep-seated  
24  
25 501 gravitational slope deformation rather than neotectonic activity. Soft-sediment  
26  
27 502 deformation structures of Lateglacial or early Holocene age at sites in western  
28  
29 503 Scotland have been inferred to relate to  $M \approx 4.6$ – $6.4$  earthquakes, though some may  
30  
31 504 have been triggered by catastrophic drainage of glacial lakes rather than crustal uplift  
32  
33 505 (Davenport and Ringrose, 1987; Ringrose 1989a, 1989b; Fenton, 1992; Stewart *et al.*,  
34  
35 506 2001). The available evidence appears compatible with enhanced Lateglacial and  
36  
37 507 early Holocene seismicity in Scotland due to glacio-isostatic crustal rebound, but the  
38  
39 508 magnitude of earthquake activity at this time remains uncertain (Firth and Stewart,  
40  
41 509 2000).

42  
43  
44  
45  
46  
47 510  
48 511 For a site at Arisaig in Western Scotland (110 km north of the Paps of Jura), Firth and  
49  
50 512 Stewart (2000) derived rates of crustal uplift based on a sea-level curve produced by  
51  
52 513 Shennan *et al.* (1995). Their data show that the maximum averaged rates of uplift  
53  
54 514 (14.3–26.7 mm a<sup>-1</sup>) occurred during the period ~15.7–12.7 ka, then dropped to  
55  
56 515 ~12.9 mm a<sup>-1</sup> during ~12.7–10.7 ka and ~4.2 mm a<sup>-1</sup> within the period ~10.7–7.1 ka.

1  
2  
3 516 The inferred Lateglacial timing of the Jura RSFs coincides with the period of most  
4  
5 517 rapid crustal uplift (Figure 7), suggesting that the two may be linked through seismic  
6  
7 518 triggering of failure by uplift-induced earthquake activity. Such low-resolution temporal  
8  
9 519 coincidence is not proof of causation, but suggests that the role of uplift-driven  
10  
11 520 seismicity in triggering paraglacial RSFs in Scotland, downplayed in some recent  
12  
13 521 studies (Jarman, 2006; Ballantyne and Stone, 2013), requires re-evaluation.  
14  
15

### 16 522 17 523 **Comparisons and implications**

18  
19 524  
20 525 Our results accord closely with exposure ages obtained from 14 other RSF sites that  
21  
22 526 were deglaciated during retreat of the last British-Irish Ice Sheet but escaped glacial  
23  
24 527 reoccupance during the LLS of ~12.9–11.7 ka. Nine exposure-dated RSF runout  
25  
26 528 deposits at the foot of quartzite mountains in NW Ireland produced ages of  
27  
28 529  $17.7 \pm 0.9$  ka to  $12.5 \pm 0.7$  ka (LL LPR) or  $16.3 \pm 0.7$  ka to  $11.7 \pm 0.5$  ka (NWH11.6  
29  
30 530 LPR), implying that all RSFs in this area occurred in the interval between deglaciation  
31  
32 531 and the beginning of the Holocene at ~11.7 ka (Ballantyne *et al.*, 2013). Similarly, five  
33  
34 532 RSF runout deposits on granite and sandstone mountains in the Scottish Highlands  
35  
36 533 yielded ages ranging from ~16.9 ka to ~12.8 ka (Ballantyne and Stone, 2013). For  
37  
38 534 areas that lay outside the limits of LLS glaciation only one dated RSF has produced  
39  
40 535 an unequivocal Holocene age: a major rockslide of basalt lavas, probably seated on  
41  
42 536 underlying shale, that occurred on the Isle of Skye at ~6.1 ka (Ballantyne *et al.*, 1998).  
43  
44 537 Excluding this single exception (and possibly the BCW and/or BOE RSFs on Jura), all  
45  
46 538 20 dated RSFs outside the limits of LLS glaciation in the British Isles appear to have  
47  
48 539 occurred between ice-sheet deglaciation and the beginning of the Holocene. This  
49  
50 540 implies that the great majority of undated RSFs in British and Irish mountains outside  
51  
52 541 the limits of LLS (Younger Dryas) glaciation also occurred during the Lateglacial  
53  
54 542 period, within a few millennia of ice-sheet deglaciation  
55  
56  
57  
58  
59  
60

1  
2  
3 543  
4 544 During the Lateglacial Interstade of ~14.7–12.9 ka (Figure 7), glacier ice completely  
5  
6 545 disappeared from upland Britain or survived only in favoured locations such as cirques  
7  
8 546 or high plateaux (Finlayson *et al.*, 2011; Ballantyne and Stone 2012; Fabel *et al.*,  
9  
10 547 2012). The ensuing LLS of ~12.9–11.7 ka was a period of full-stadial climate during  
11  
12 548 which glacier ice expanded to form a major icefield in the Western Highlands  
13  
14 549 (Golledge, 2010), with peripheral icefields and numerous smaller glaciers in the  
15  
16 550 Hebrides, northern Scotland, the eastern Grampians, English Lake District, NW Wales  
17  
18 551 and the mountains of Ireland. As almost all dated RSFs that occur outside the limit of  
19  
20 552 LLS glaciation occurred prior to the onset of the LLS, an interesting implication is that  
21  
22 553 numerous Lateglacial RSFs presumably also occurred within areas reoccupied by  
23  
24 554 glacier ice during the LLS but have not been recorded because RSF runout debris  
25  
26 555 was removed by glaciers. Some of this ‘lost generation’ of Lateglacial RSFs may be  
27  
28 556 identified from the morphology of failure scars, particularly where these are located  
29  
30 557 above the upper limits of LLS glacier ice. Diagnostic criteria for such sites include  
31  
32 558 steep headscarps separated by a break of slope from a subjacent failure plane, flank  
33  
34 559 scarps, and tension cracks or detached blocks near the headscarp (Ballantyne, 2013).  
35  
36 560 Implications of these debris-free Lateglacial RSF scars are: (1) that RSF inventories  
37  
38 561 based on RSF runout or displaced rock masses (e.g. Jarman, 2006) underestimate  
39  
40 562 the number of RSFs since ice-sheet deglaciation; (2) that RSFs may have played a  
41  
42 563 more important role in the evolution of valley-side slopes and cirque evolution in  
43  
44 564 upland Britain than has hitherto been appreciated; and (3) that RSFs probably made a  
45  
46 565 significant contribution to the sediment budget of Younger Dryas glaciers in the British  
47  
48 566 Isles, locally manifest in the form of exceptionally large end moraines and suites of  
49  
50 567 hummocky recessional moraines (Ballantyne, 2013).  
51  
52  
53  
54  
55  
56  
57 568  
58 569  
59  
60

1  
2  
3 570 More generally, the results from this study and those of Ballantyne and Stone (2013)  
4  
5 571 and Ballantyne *et al.* (2013) support the conclusions of previous work in Scandinavia  
6  
7 572 (Blikra *et al.*, 2006; Longva *et al.*, 2009), Iceland (Mercier *et al.*, 2013) and the Andes  
8  
9 573 (Fauqué *et al.*, 2009) indicating a period of enhanced Lateglacial and early Holocene  
10  
11 574 RSF activity following ice-sheet retreat, even though it is clear that many dated  
12  
13 575 postglacial RSFs (particularly in tectonically active mountain belts) occurred several  
14  
15 576 millennia after Late Pleistocene or early Holocene deglaciation (Hewitt *et al.*, 2008;  
16  
17 577 McColl, 2012). It seems reasonable to conclude that in intraplate areas of relative  
18  
19 578 (present-day) tectonic stability, such as Scotland and Fennoscandia, paraglacial  
20  
21 579 stress release and consequent fracture propagation have played a key role in  
22  
23 580 preconditioning Lateglacial or early Holocene failures and that seismotectonic activity  
24  
25 581 related to glacio-isostatic uplift probably triggered kinematic release in many cases.  
26  
27  
28  
29

## 30 582 **Conclusions**

31 583  
32  
33 584 <sup>10</sup>Be exposure ages obtained on the runout debris of five postglacial rock-slope  
34 585 failures seated on the quartzite mountains of Jura demonstrate that at least three and  
35  
36 586 probably all five occurred during the Late Devensian Lateglacial period, between 15.4  
37  
38 587 ± 0.9 ka and 12.8 ± 0.6 ka, though we cannot exclude a possible later age (~12–8 ka)  
39  
40 588 for two of these. Comparison with a deglaciation age based on <sup>10</sup>Be exposure dating  
41  
42 589 of a nearby medial moraine shows that all five dated RSFs occurred at least 770–2240  
43  
44 590 years after deglaciation, implying that removal of ice during deglaciation  
45  
46 591 (debuttressing) played no role in directly triggering failure at these sites. The RSF that  
47  
48 592 apparently sourced the debris in the medial moraine, however, must have occurred as  
49  
50 593 the last ice sheet downwasted below the level of the summits, and may represent a  
51  
52 594 direct response to the removal of the support of adjacent glacier ice. Thaw of  
53  
54 595 permafrost ice in ice-bonded rock joints seems unlikely to be implicated in failure of  
55  
56 596  
57  
58  
59  
60

1  
2  
3 597 the dated RSFs, all of which pre-date or post-date (by several centuries) the rapid  
4  
5 598 warming that occurred during the stadial-interstadial transition at ~14.7 ka.

6  
7 599  
8 600 Paraglacial stress release due to deglacial unloading and/or reduction of confining  
9  
10 601 stress is inferred to have contributed to rock-mass weakening through fracture  
11  
12 602 propagation, and it is possible that all the dated RSFs reflect time-dependent release  
13  
14 603 of strain energy, manifest through progressive development of failure planes, without  
15  
16 604 recourse to a specific triggering mechanism. However, the timing of the dated RSFs  
17  
18 605 on Jura coincides with the period of maximum glacio-isostatic crustal uplift on the west  
19  
20 606 coast of the Scottish mainland, suggesting that the two may be linked through  
21  
22 607 triggering of the Jura RSFs by uplift-driven seismic events acting on rock slopes  
23  
24 608 weakened by stress release and associated fracture propagation.

25  
26  
27  
28 609  
29 610 Our results have several wider implications. The inferred Lateglacial timing of all dated  
30  
31 611 RSFs on Jura contributes to growing evidence for a period of greatly enhanced RSF  
32  
33 612 activity within a few millennia following ice-sheet retreat on intraplate terrains of  
34  
35 613 relative (present-day) tectonic stability (e.g. Blikra *et al.*, 2006; Longva *et al.*, 2009;  
36  
37 614 Ballantyne and Stone, 2013; Ballantyne *et al.*, 2013). In particular, the timing of the  
38  
39 615 Jura RSFs is consistent with the proposition that such enhanced Lateglacial RSF  
40  
41 616 activity reflects triggering of failure by earthquakes associated with fault movements  
42  
43 617 driven by rapid glacio-isostatic uplift over a period of a few millennia following ice-  
44  
45 618 sheet retreat (e.g. Lagerbäck, 1992; Mörner, 1991, 2004; Mörner *et al.*, 2000; Mercier  
46  
47 619 *et al.*, 2013; Cossart *et al.*, 2013). Exposure dating of postglacial fault scarps (cf.  
48  
49 620 Sanchez *et al.*, (2010) may help confirm the temporal connections between uplift,  
50  
51 621 palaeoseismicity and enhanced RSF activity following ice-sheet deglaciation  
52  
53  
54  
55

56 622  
57 623  
58  
59  
60



1  
2  
3 624 More locally, comparison of the results reported here with those other studies devoted  
4  
5 625 to dating of RSFs in the British Isles (Ballantyne and Stone, 2013; Ballantyne *et al.*,  
6  
7 626 2013) shows that almost all dated RSFs located outside the limits of LLS glaciers  
8  
9 627 occurred before the beginning of the Holocene at ~11.7 ka, implying that the great  
10  
11 628 majority of undated RSFs in such areas are also of Lateglacial age, and suggesting  
12  
13 629 that the risk of future major RSFs in such areas is extremely low. Enhanced  
14  
15 630 Lateglacial RSF activity outside the LLS glacial limits also implies that numerous RSFs  
16  
17 631 must also have occurred inside these limits during the interval between ice-sheet  
18  
19 632 retreat and the end of the LLS at ~11.7 ka, but as the runout debris from such RSFs  
20  
21 633 has been removed by LLS glaciers, are represented only by failure scars (Ballantyne,  
22  
23 634 2013). Identification of such 'empty' RSF source areas and assessment of their  
24  
25 635 implications for long-term development of mountain form and the sediment budget of  
26  
27 636 LLS glaciers represent interesting topics for further research.  
28  
29  
30  
31

### 32 637 **Acknowledgements** 33 638

34  
35 639 This research was supported by the NERC Cosmogenic Isotope Analysis Facility  
36 640 through award of sample preparation and analysis (CIAF project 9046.0308) and by a  
37  
38 641 grant from the British Society for Geomorphology in support of the cost of fieldwork on  
39  
40 642 Jura. We thank Dr Derek Fabel of the University of Glasgow and Dr John Stone of the  
41  
42 643 University of Washington for permission to use <sup>10</sup>Be calibration datasets in advance of  
43  
44 644 publication. We also thank Sheng Xu and Dylan Rood (SUERC) for carrying out the  
45  
46 645 AMS measurements and Graeme Sandeman (University of St Andrews) for drafting  
47  
48 646 the figures.  
49  
50  
51 647  
52  
53  
54 648  
55 649  
56  
57  
58  
59  
60

## References

- 650  
651  
652 Abele G. 1974. *Bergstürze in den Alpen: Ihre Verbreitung, Morphologie und*  
653 *Folgeerscheinungen*. Deutscher und Österreichischer Alpenverein, Munich.
- 654 Agliardi F, Crosta GB, Zanchi A, Ravazzi C. 2009. Onset and timing of deep-seated  
655 gravitational slope deformations in the eastern Alps, Italy. *Geomorphology* **103**:  
656 113–129. DOI: 10.1016/j.geomorph.2007.09.015.
- 657 Allen S, Cox S, Owens I. 2010. Rock avalanches and other landslides in the central  
658 Southern Alps of New Zealand: a regional study considering possible climate  
659 change impacts. *Landslides* **8**: 33–48. DOI: 10.1007/s10346-010-0222-z.
- 660 Amadei B, Stephansson O. 1997. *Rock Stress and its Measurement*. Chapman and  
661 Hall, London.
- 662 Antinao JL, Gosse J. 2009. Large rockslides in the southern central Andes of Chile  
663 (32–34.5°S): tectonic control and significance for Quaternary landscape evolution.  
664 *Geomorphology* **104**: 117–133. DOI: 10.1016/j.geomorph.2008.08.008.
- 665 Anderton R. 1976. Tidal shelf sedimentation: an example from the Scottish Dalradian.  
666 *Sedimentology* **23**: 42–458.
- 667 Anderton R. 1977. The Dalradian rocks of Jura. *Scottish Journal of Geology* **13**: 135–  
668 142.
- 669 Anderton R. 1985. Sedimentation and tectonics in the Scottish Dalradian. *Scottish*  
670 *Journal of Geology* **21**: 407–436.
- 671 Arsenault AM, Meigs AJ. 2005. Contribution of deep-seated bedrock landslides to  
672 erosion of a glaciated basin in southern Alaska. *Earth Surface Processes and*  
673 *Landforms* **30**: 1111–1125. DOI: 10.1002/esp1265.
- 674 Atkinson TC, Briffa KR, Coope GR. 1987. Seasonal temperatures in Britain during the  
675 past 22,000 years, reconstructed using beetle remains. *Nature* **325**: 587–592.
- 676 Augustinus PC. 1995. Glacial valley cross-profile development: the influence of in situ  
677 rock stress and rock mass strength, with examples from the Southern Alps, New  
678 Zealand. *Geomorphology* **14**: 87–97.
- 679 Balco G. 2011. Contributions and unrealized potential contributions of cosmogenic-  
680 nuclide exposure dating to glacier chronology, 1990–2010. *Quaternary Science*

- 1  
2  
3 681 *Reviews* **30**: 3–27. DOI: 10.1016/j.quascirev.2010.11.003
- 4  
5 682 Balco G, Briner J, Finkel RC, Rayburn JA, Ridge JC, Schaefer JM. 2009. Regional  
6 683 beryllium-10 production rate calibration for late-glacial northeastern North America.  
7 684 *Quaternary Geochronology* **4**: 93–107. DOI: 10.1016/j.quageo.2008.09.001
- 8  
9  
10 685 Balco G, Stone JO, Lifton NA, Dunai TJ. 2008. A complete and easily accessible  
11 686 means of calculating surface exposure ages or erosion rates from <sup>10</sup>Be and <sup>26</sup>Al  
12 687 measurements. *Quaternary Geochronology* **3**: 174–195. DOI:  
13 688 10.1016/j.quageo.2007.12.001.
- 14  
15  
16  
17 689 Ballantyne CK. 1992. Rock slope failure and debris flow, Gleann na Guiseran,  
18 690 Knoydart. *Scottish Journal of Geology* **28**: 77–80.
- 19  
20  
21 691 Ballantyne CK. 1997. Holocene rock-slope failures in the Scottish Highlands.  
22 692 *Paläoklimaforschung* **19**: 197–206.
- 23  
24  
25 693 Ballantyne CK. 1999. Maximum altitude of Late Devensian glaciation on the Isle of  
26 694 Mull and Isle of Jura. *Scottish Journal of Geology* **35**: 97–106.
- 27  
28  
29 695 Ballantyne CK. 2002. Paraglacial geomorphology. *Quaternary Science Reviews* **21**:  
30 696 1935–2017.
- 31  
32  
33 697 Ballantyne CK. 2007. Carn Dubh, Ben Gulabin, Perthshire. In *Mass Movements in*  
34 698 *Great Britain*, Cooper R (ed). Geological Conservation Review Series, No. 33, Joint  
35 699 Nature Conservation Committee, Peterborough; 107–111.
- 36  
37  
38 700 Ballantyne CK. 2010. Extent and deglacial chronology of the last British-Irish ice  
39 701 sheet: implications of exposure dating using cosmogenic isotopes. *Journal of*  
40 702 *Quaternary Science* **25**: 515–534. DOI:10.1002/jqs.1310.
- 41  
42  
43 703 Ballantyne CK 2013. Lateglacial rock-slope failures in the Scottish Highlands. *Scottish*  
44 704 *Geographical Journal* **129**: 67–84. DOI: 10.1080/14702541.2013.781210.
- 45  
46  
47 705 Ballantyne CK, Harris C. 1994. *The Periglaciation of Great Britain*. Cambridge  
48 706 University Press: Cambridge.
- 49  
50  
51 707 Ballantyne CK, Stone JO. 2009. Rock-slope failure at Baosbheinn, Wester Ross, NW  
52 708 Scotland: age and interpretation. *Scottish Journal of Geology* **45**: 177–181. DOI:  
53 709 10.114/0036-9276/01-388.
- 54  
55  
56  
57 710 Ballantyne CK, Stone JO. 2012. Did large ice caps persist on low ground in north-west  
58  
59  
60

- 1  
2  
3 711 Scotland during the Lateglacial Interstade? *Journal of Quaternary Science* **27**: 297–  
4 712 306. DOI: 10.1002/jqs.1544.
- 5  
6 713 Ballantyne CK, Stone JO. 2013. Timing and periodicity of paraglacial rock-slope  
7 714 failures in the Scottish Highlands. *Geomorphology* **186**: 150–161. DOI:  
8 715 10.1016/j.geomorph.2012.12.030.
- 9  
10 716 Ballantyne CK, Stone JO, Fifield LK. 1998. Cosmogenic <sup>36</sup>Cl dating of postglacial  
11 717 landsliding at The Storr, Isle of Skye, Scotland. *The Holocene* **8**: 347–351.
- 12  
13 718 Ballantyne CK, Wilson P, Schnabel C, Xu S. 2013. Lateglacial rock-slope failures in  
14 719 NW Ireland: age, causes and implications. *Journal of Quaternary Science* (in  
15 720 press).
- 16  
17 721 Barnard P, Owen LA, Sharma MC, Finkel RC. 2001. Natural and human-induced  
18 722 landsliding in the Garhwal Himalaya of northern India. *Geomorphology* **40**: 21–35.
- 19  
20 723 Bigot-Cormier F, Braucher R, Bourlès D, Guglielmi Y, Dubar M, Stéphan J-F. 2005.  
21 724 Chronological constraints on processes leading to large landslides. *Earth and*  
22 725 *Planetary Science Letters* **235**: 141–150. DOI: 10.1016/j.epsl.2005.03.012.
- 23  
24 726 Blikra LH, Longva O, Braathen A, Dehls JF, Stalsberg K. 2006. Rock slope failures in  
25 727 Norwegian Fjord areas: examples, spatial distribution and temporal pattern. In  
26 728 *Landslides from massive rock slope failure*, Evans SG, Mugnozza GS, Strom A,  
27 729 Hermanns RL. (eds). Springer, Dordrecht, 475–496.
- 28  
29 730 Brideau M-A, Yan M, Stead D. 2009. The role of tectonic damage and brittle rock  
30 731 failure in the development of large rock failures. *Geomorphology* **103**: 30–49. DOI:  
31 732 10.1016/j.geomorph.2008.04.010.
- 32  
33 733 Brooks SJ, Birks HJB. 2000. Chironomid-inferred Late-glacial air temperatures at  
34 734 Whitrig Bog, southeast Scotland. *Journal of Quaternary Science* **15**: 759–764.
- 35  
36 735 Brooks SJ, Matthews IP, Birks HH, Birks HJB. 2012. High resolution Lateglacial and  
37 736 early-Holocene summer air temperature records from Scotland inferred from  
38 737 chironomid assemblages. *Quaternary Science Reviews* **41**: 67–82. DOI:  
39 738 10.1016.quascirev.2012.03.007.
- 40  
41 739 Child D, Elliott G, Mifsud C, Smith A, Fink D. 2000. Sample processing for earth  
42 740 science studies at ANTARES. *Nuclear Instruments and Methods in Physics*  
43 741 *Research* **B172**: 856–860.
- 44  
45  
46  
47  
48  
49  
50  
51  
52  
53  
54  
55  
56  
57  
58  
59  
60

- 1  
2  
3 742 Clark CD, Hughes ALC, Greenwood SL, Jordan C, Sejrup HP. 2012. Pattern and  
4 743 timing of retreat of the last British-Irish Ice Sheet. *Quaternary Science Reviews* **44**:  
5 744 112–146. DOI: 10.1016/j.quascirev.2010.07.019.
- 6  
7  
8 745 Cossart E, Braucher R, Fort M, Bourlès DL, Carcaillet J. 2008. Slope instability in  
9 746 relation to glacial debuitressing in alpine areas (Upper Durance catchment,  
10 747 southeastern France): evidence from field data and <sup>10</sup>Be cosmic ray exposure ages.  
11 748 *Geomorphology* **95**: 3–26. DOI:10.1016/j.geomorph.2006.12.022.
- 12  
13  
14  
15 749 Cossart E, Mercier D, Decaulne A, Feuillet T, Jónsson HP, Sæmundsson, Þ. 2013.  
16 750 Impacts of post-glacial rebound on landslide spatial distribution at a regional scale  
17 751 in northern Iceland (Skagafjörður). *Earth Surface Processes and Landforms*. DOI:  
18 752 10.1002/esp.3450.
- 19  
20  
21  
22 753 Cruden D, Hu XQ. 1993. Exhaustion and steady state models for predicting landslide  
23 754 hazards in the Canadian Rocky Mountains. *Geomorphology* **8**: 279–285.
- 24  
25  
26 755 Davenport CA, Ringrose PS. 1987. Deformation of Scottish Quaternary sediment  
27 756 sequences by strong earthquake motions. *Geological Society Special Publication*  
28 757 **29**: 299–314.
- 29  
30  
31  
32 758 Davenport CA, Ringrose PS, Becker A, Hancock P, Fenton C. 1989. Geological  
33 759 investigations of Late- and Postglacial earthquake activity in Scotland. In  
34 760 *Earthquakes at North Atlantic passive margins: neotectonics and postglacial*  
35 761 *rebound*, Gregersen S, Basham P. (eds.) Kluwer, Dordrecht, 175–194.
- 36  
37  
38  
39 762 Davies MCR, Hamza O, Harris C. 2001. The effect of rise in mean annual temperature  
40 763 on the stability of rock slopes containing ice-filled discontinuities. *Permafrost and*  
41 764 *Periglacial Processes* **12**: 137–144.
- 42  
43  
44 765 Dawson AG. 1977. A fossil rock glacier in Jura. *Scottish Journal of Geology* **13**: 37–  
45 766 41.
- 46  
47  
48 767 Dawson AG. 1979. A Devensian medial moraine in Jura. *Scottish Journal of Geology*  
49 768 **15**: 43–48.
- 50  
51  
52 769 Dortch JM, Owen LA, Haneberg WC, Caffee MW, Dietsch C, Kamp U, 2009. Nature  
53 770 and timing of large landslides in the Himalaya and Transhimalaya of northern India.  
54 771 *Quaternary Science Reviews* **28**: 1037–1054. DOI: 10.1016/quascirev.2008.05.002.
- 55  
56  
57  
58 772 Eberhardt E, Stead D, Coggan JS. 2004. Numerical analysis of initiation and  
59  
60

- 1  
2  
3 773 progressive failure in natural rock slopes – the 1991 Randa rockslide. *International*  
4 774 *Journal of Rock Mechanics and Mining Science* **41**: 69–87.
- 5  
6  
7 775 El Bedoui S, Gugliemi Y, Lebourg T, Pérez J-L. 2009. Deep-seated failure  
8 776 propagation in a fractured rock slope over 10,000 years: the La Clapière slope, the  
9  
10 777 south-eastern French Alps. *Geomorphology* **105**: 232–238. DOI:  
11 778 10.1016/j.geomorph.2008.0.025.
- 12  
13  
14 779 Evans SG, Clague JJ. 1994. Recent climate change and catastrophic geomorphic  
15 780 processes in mountain environments. *Geomorphology* **10**: 107–128.
- 16  
17  
18 781 Fabel D, Ballantyne CK, Xu S. 2012. Trimlines, blockfields, mountain-top erratics and  
19 782 the vertical dimensions of the last British-Irish Ice Sheet in NW Scotland. *Quaternary*  
20 783 *Science Reviews* **55**: 91–102. DOI: 10.1016/j.quascirev.2012.09.002.
- 21  
22  
23 784 Fauqué L, Hermanns RL, Hewitt K, Rosas M, Wilson C, Baumann V, Lagorio S, Di  
24 785 Tommaso I. 2009. Mega-deslizamientos de la pared sur del Cerro Aconcagua y su  
25 786 relación con depósitos asignados a la glaciación Pleistocena. *Revista de la*  
26 787 *Asociación Geológica Argentina* **65**: 691–712.
- 27  
28  
29  
30 788 Fenton CH (ed). 1992. *Neotectonics in Scotland: a field guide*. University of Glasgow:  
31 789 Glasgow.
- 32  
33  
34 790 Finlayson A, Golledge N, Bradwell T, Fabel D. 2011. Evolution of a Lateglacial  
35 791 mountain icecap in northern Scotland. *Boreas* **40**: 536–554. DOI: 10.1111/j.1502-  
36 792 3885.2010.00202.x.
- 37  
38  
39 793 Firth CR, Stewart IS. 2000. Postglacial tectonics of the Scottish glacio-isostatic uplift  
40 794 centre. *Quaternary Science Reviews* **19**: 1469–1493.
- 41  
42  
43 795 Golledge NR. 2010. Glaciation of Scotland during the Younger Dryas Stadial: a  
44 796 review. *Journal of Quaternary Science* **25**: 550–566. DOI: 10.1002/jqs.1319.
- 45  
46  
47 797 Gregerson S, Basham PW. (eds.) 1989. *Earthquakes at North Atlantic passive*  
48 798 *margins: neotectonics and postglacial rebound*. Kluwer: Dordrecht.
- 49  
50  
51 799 Gruber S, Haeberli W. 2007. Permafrost in steep bedrock slopes and its temperature-  
52 800 related destabilization following climate change. *Journal of Geophysical Research*  
53 801 **112**: F02S18. DOI: 10.1029/2006JF000547.
- 54  
55  
56 802 Gugliemi Y, Cappa F. 2010. Regional-scale relief evolution and large landslides:  
57 803 insights from geomechanical analyses in the Tinée Valley (southern French Alps).

- 1  
2  
3 804 *Geomorphology* **117**: 121–129. DOI: j.geomorph.2009.11.016.
- 4  
5 805 Haeberli W, Wegmann M, Vonder Mühl D. 2008. Slope stability problems related to  
6 806 glacier shrinkage and permafrost degradation in the Alps. *Eclogae Geologicae*  
7 807 *Helveticae* **90**: 407–414.
- 8  
9  
10 808 Hermanns RL, Niedermann, S. 2011. Late Pleistocene–early Holocene  
11 809 palaeoseismicity deduced from lake sediment deformation and coeval landsliding in  
12 810 the Calchaquies valleys, NW Argentina. *Geological Society of America Special*  
13 811 *Paper* **479**: 181–194. DOI: 10.1130/2011.2479(08).
- 14  
15  
16  
17 812 Hermanns RL, Schellenberger, A. 2008. Quaternary tephrochronology helps define  
18 813 conditioning factors and triggering mechanisms of rock avalanches in NW Argentina.  
19 814 *Quaternary International* **178**: 261–275. DOI: 10.1016/j.quaint.2007.05.002.
- 20  
21  
22  
23 815 Hermanns RL, Redfield TF, Bunkholt HSS, Fischer L, Oppikofer T. 2012. Cosmogenic  
24 816 nuclide dating of slow-moving rockslides in Norway in order to assess long-term  
25 817 slide velocities. In *Landslides and engineered slopes: protecting society through*  
26 818 *improved understanding*, Eberhardt E, Froese C, Turner K, Leroueil S (eds). CRC  
27 819 Press: Boca Raton; 84-854.
- 28  
29  
30  
31 820 Hewitt K, Clague JJ, Orwin, JF. 2008. Legacies of catastrophic rock slope failures in  
32 821 mountain landscapes. *Earth-Science Reviews* **87**: 1–38. DOI:  
33 822 10.1016/j.earscirev.2007.10.1002.
- 34  
35  
36  
37 823 Hewitt K, Gosse J, Clague JJ. 2011. Rock avalanches and the pace of Late  
38 824 Quaternary development of river valleys in the Karakoram Himalaya. *Geological*  
39 825 *Society of America Bulletin* **123**: 1836–1850. DOI: 10.1130/B30341.1.
- 40  
41  
42  
43 826 Hencher SR, Lee SG, Carter TG, Richards LR. 2011. Sheeting joints: characterisation,  
44 827 shear strength and engineering. *Rock Mechanics and Rock Engineering* **44**: 1-22.  
45 828 DOI: 10.1007/s00603-010-0100-y.
- 46  
47  
48 829 Heyman J, Stroeven AP, Harbor JM, Caffee MW. 2011. Too young or too old:  
49 830 evaluating cosmogenic exposure dating based on an analysis of compiled boulder  
50 831 exposure ages. *Earth and Planetary Science Letters* **302**: 71–80. DOI:  
51 832 10.1016/j.epsl.2010.11.040.
- 52  
53  
54  
55 833 Hippolyte J-C, Bourlès D, Braucher R, Carcaillet J, Léanni L, Arnold M, Aumaître G.  
56 834 2009. Cosmogenic <sup>10</sup>Be dating of a sackung and its faulted rock glaciers, in the

- 1  
2  
3 835 Alps of Savoy (France). *Geomorphology* **108**: 312–320. DOI:  
4 836 10.1016/j.geomorph.200.02.024.  
5  
6  
7 837 Hormes A, Ivy-Ochs S, Kubik PW, Ferreli L, Michetti AM. 2008.  $^{10}\text{Be}$  exposure ages of  
8 838 a rock avalanche and a late glacial moraine in the Alta Valtellina, Italian Alps.  
9  
10 839 *Quaternary International* **190**: 136–145. DOI: 10.1016/j.quaint.2007.06.036.  
11  
12 840 Hubbard A, Bradwell T, Golledge NR, Hall AM, Patton H, Sugden DE, Cooper R,  
13 841 Stoker MS. 2009. Dynamic cycles, ice streams and their impact on the extent,  
14 842 chronology and deglaciation of the British-Irish Ice Sheet. *Quaternary Science*  
15 843 *Reviews* **28**: 758–776. DOI: 10.1016/j.quascirev.2008.12.026.  
16  
17  
18  
19 844 Ivy-Ochs, S., Schaller, M., 2010. Examining processes and rates of landscape change  
20 845 with cosmogenic radionuclides. *Radioactivity in the Environment* **16**: 231–294.  
21  
22  
23 846 Ivy-Ochs, S., Poschinger, A.V., Synal, H-A., Maisch, M., 2009. Surface exposure  
24 847 dating of the Flims landslide, Graubünden, Switzerland. *Geomorphology* **103**: 104–  
25 848 112. DOI: 10.1016/j.geomorph.2007.10.024.  
26  
27  
28  
29 849 Jarman D. 2006. Large rock-slope failures in the Highlands of Scotland:  
30 850 characterisation, causes and spatial distribution. *Engineering Geology* **83**: 161–182.  
31 851 DOI: 10.1016/j.enggeo.2005.06.030.  
32  
33  
34 852 Jarman D, Wilson P, Harrison S. 2013. Are there any relict rock glaciers in the British  
35 853 mountains? *Journal of Quaternary Science* **28**: 131–143. DOI: 10.1002/jqs.2574.  
36  
37  
38 854 Kaplan MR, Schaefer JM, Denton GH, Barrell DJA, Chinn TJH, Putnam AE, Andersen  
39 855 BG, Finkel RC, Schwartz R, Doughty AM. 2010. Glacier retreat in New Zealand  
40 856 during the Younger Dryas stadial. *Nature* **467**: 194–197. DOI:  
41 857 10.1038/nature09313.  
42  
43  
44  
45 858 Kemeny J. 2003. The time-dependent reduction of sliding cohesion due to rock  
46 859 bridges along discontinuities: a fracture mechanics approach. *Rock Mechanics and*  
47 860 *Rock Engineering* **36**: 27–38.  
48  
49  
50  
51 861 Kohl C, Nishiizumi K. 1992. Chemical isolation of quartz for measurement of in situ-  
52 862 produced cosmogenic nuclides. *Geochimica et Cosmochimica Acta* **56**: 3586–3587.  
53  
54  
55 863 Krautblatter M, Funk D, Günzel FK. 2013. Why permafrost rocks become unstable: a  
56 864 rock-ice-mechanical model in space and time. *Earth Surface Processes and*  
57 865 *Landforms* DOI: 10.1002/esp3374.  
58  
59  
60



- 1  
2  
3 866 Krautblatter M, Huggel C, Deline P, Hasler A. 2012. Research perspectives on  
4 867 unstable high-alpine bedrock permafrost: measurement, modelling and process  
5 understanding. *Permafrost and Periglacial Processes* **23**: 80–88. DOI:  
6 868 10.1002/ppp.740.  
7 869
- 8  
9  
10 870 Lagerbäck, R. 1992. Dating of Late Quaternary faulting in northern Sweden. *Journal of*  
11 871 *the Geological Society, London* **149**: 285-291.
- 12  
13  
14 872 Lal D. 1991. Cosmic ray labeling of erosion surfaces: in situ nuclide production rates  
15 and erosion models. *Earth and Planetary Science Letters* **104**: 424–439.  
16 873
- 17  
18 874 Leith K, Amann F, Moore JR, Kos A, Loew S. 2010. Conceptual modelling of near-  
19 875 surface extensional fracture in the Matter and Saas Valleys, Switzerland. In  
20 876 *Geologically Active. Proceedings of the 11th IAEG Congress, Auckland, New*  
21 877 *Zealand*, Williams AL, Pinches GM, Chin CY, McMorran TJ, Massey CI (eds). CRC  
22 878 Press, Boca Raton; 363–371.
- 23  
24  
25  
26 879 Leith K, Moore J, Amann F, Loew S. 2011. Effect of glacial ice cover on fracturing  
27 880 critically stressed bedrock. *Geophysical Research Abstracts* **13**: EGU2011-12825-  
28 881 2.
- 29  
30  
31  
32 882 Longva O, Blikra LH, Dehls JF. 2009. Rock avalanches: distribution and frequencies  
33 883 in the inner part of Storfjorden, Møre og Romsdal County, Norway. *Geological*  
34 884 *Survey of Norway, Report* 2009.002, 32 pp.
- 35  
36  
37 885 Lowe JJ, Rasmussen SO, Björk S, Hoek WJ, Steffensen JP, Walker MJC, Yu ZC,  
38 886 INTIMATE Group. 2008. Synchronisation of palaeoenvironmental events in the  
39 887 North Atlantic region during the Last Termination: a revised protocol recommended  
40 888 by the INTIMATE Group. *Quaternary Science Reviews* **27**: 6–17. DOI:  
41 889 10.1016/j.quascirev.2007.09.016.
- 42  
43  
44  
45  
46 890 MacLeod A, Palmer AP., Lowe JJ, Rose J, Bryant C., Merritt J. 2011. Timing of glacier  
47 891 response to Younger Dryas climatic cooling in Scotland. *Global and Planetary*  
48 892 *Change* **79**: 264–274. DOI: 10.1016/j.gloplacha.2010.07.006.
- 49  
50  
51 893 McColl ST. 2012. Paraglacial rock-slope stability. *Geomorphology* **153-154**: 1–16.  
52 894 DOI: 10.1016/j.geomorph.2012.02.015.
- 53  
54  
55  
56 895 Mercier D., Cossart E., Decaulne A, Feuillet T, Jónsson HP, Sæmundsson Þ. 2013.  
57 896 The Höfðahólar rock avalanche (sturzstrom): chronological constraint of paraglacial

- 1  
2  
3 897      landsliding on an Icelandic hillslope. *The Holocene* **23**: 432-446. DOI:  
4 898      10.1177/0959683612463014.
- 5  
6  
7 899      Mitchell WA, McSaveney MJ, Zundervan A, Kim K, Dunning SA, Taylor PJ. 2007. The  
8 900      Keylong Serai rock avalanche, NW Indian Himalaya: geomorphology and  
9 901      palaeoseismic implications. *Landslides* **4**: 245–254. DOI: 10.1007/s10346-007-  
10 902      0085-0.
- 11  
12  
13  
14 903      Mörner N-A. 1991. Intense earthquakes and seismotectonics as a function of glacial  
15 904      isostasy. *Tectonophysics* **188**: 407–410.
- 16  
17  
18 905      Mörner N-A. 2004. Active faults and palaeoseismicity in Fennoscandia, especially  
19 906      Sweden. Primary structure and secondary effects. *Tectonophysics* **380**: 139–157.  
20 907      DOI: 10.1016/j.tecto.2003.09.015.
- 21  
22  
23 908      Mörner N-A. 2005. An interpretation and catalogue of palaeoseismicity in Sweden.  
24 909      *Tectonophysics* **408**: 265–307. DOI: 10.1016/j.tecto.2005.05.039.
- 25  
26  
27 910      Mörner, N-A, Tröften PE, Sjöberg R, Grant D, Dawson S, Bronge C, Kvamsdal O,  
28 911      Sidén A. 2000. Deglacial palaeoseismicity in Sweden: the 9663 BP Iggesund event.  
29 912      *Quaternary Science Reviews* **19**: 1461–1468.
- 30  
31  
32 913      Muir-Wood R. 2000. Deglaciation seismotectonics: a principal influence on intraplate  
33 914      seismogenesis at high latitudes. *Quaternary Science Reviews* **19**: 1399–1411.
- 34  
35  
36 915      Musson RMW. 2007. British earthquakes. *Proceedings of the Geologists' Association*  
37 916      **118**: 305-337.
- 38  
39  
40 917      Nishiizumi K, Imamura M, Caffee M, Southon JR, Finkel RC, McAninch J. 2007.  
41 918      Absolute calibration of <sup>10</sup>Be AMS standards. *Nuclear Instruments and Methods*  
42 919      **B258**: 403–413. DOI: 10.1016/j.nimb.2007.01.297.
- 43  
44  
45 920      Peacock JD. 2008. Late Devensian palaeoenvironmental changes in the sea area  
46 921      adjacent to Islay, SW Scotland: implications for deglacial history of the island.  
47 922      *Scottish Journal of Geology* **44**: 183–190. DOI:
- 48  
49  
50  
51 923      Penna IM, Hermanns RL, Niedermann S, Folguera A. 2011. Multiple slope failures  
52 924      associated with neotectonic activity in the Southern Central Andes (37°–37°30'S),  
53 925      Patagonia, Argentina. *Geological Society of America, Bulletin* **123**: 1880–1895.  
54 926      DOI: 10.1130/B30399.1.
- 55  
56  
57  
58 927      Prager C, Ivy-Ochs S, Ostermann M, Synal H-A, Patzelt G. 2008. Geology and  
59  
60

- 1  
2  
3 928 radiometric  $^{14}\text{C}$ -,  $^{36}\text{Cl}$ - and Th-U-dating of the Fernpass rockslide (Tyrol, Austria).  
4 929 *Geomorphology* **103**: 93–103. DOI:10.1016/j.geomorph.2007.10.018.  
5  
6  
7 930 Putkonen J, Swanson T. 2003. Accuracy of cosmogenic dates for moraines.  
8 931 *Quaternary Research* **59**: 255-261.  
9  
10 932 Rasmussen SO, Andersen KK, Svensson AM, Steffensen JP, Vinther BM, Clausen  
11 933 HB, Siggaard-Andersen ML, Johnsen SJ, Larsen LB, Dahl-Jensen D, Bigler M,  
12 934 Rothlisberger R, Fischer H, Goto-Azuma K, Hansson ME, Ruth U. 2006. A new  
13 935 Greenland ice core chronology for the last glacial termination. *Journal of*  
14 936 *Geophysical Research* **111**: D06102. DOI: 10.1029/2005JD006079.  
15  
16  
17 937 Ringrose PS. 1989a. Recent fault movement and palaeoseismicity in western  
18 938 Scotland. *Tectonophysics* **163**: 305–314.  
19  
20  
21 939 Ringrose PS. 1989b. Palaeoseismic (?) liquifaction event in late Quaternary lake  
22 940 sediments at Glen Rpy, Scotland. *Terra Nova* **1**: 57–62.  
23  
24  
25 941 Ringrose PS, Hancock P, Fenton C, Davenport CA. 1991. Quaternary tectonic activity  
26 942 in Scotland. *Geological Society Engineering Geology Special Publication* **7**: 679–  
27 943 686.  
28  
29  
30 944 Sanchez G, Rolland Y, Corsini M, Braucher R, Boulès D, Arnold M, Aumaître G.  
31 945 2010. Relationships between tectonics, slope instability and climate change: cosmic  
32 946 ray exposure dating of active faults, landslides and glacial surfaces in the French  
33 947 Alps. *Geomorphology* **117**: 1–13. DOI: 10.1016/j.geomorph.200.10.019.  
34  
35  
36 948 Sanhueza-Pino K, Korup O, Hetzel R, Munack H, Weidinger JT, Dunning S, Ormukov  
37 949 C, Kubik PW. 2011. Glacial advances constrained by  $^{10}\text{Be}$  exposure dating of  
38 950 bedrock landslides, Kyrgyz Tien Shan. *Quaternary Research* **76**: 295–304. DOI:  
39 951 10.1016/j.yqres.2011.06.013.  
40  
41  
42 952 Seong YB, Bishop MP, Bush A, Clendon P, Copland L, Finkel RC, Kamp U, Owen LA,  
43 953 Schroder, JF. 2009. Landforms and landscape evolution in the Skardu, Shigar and  
44 954 Braldu Valleys, Central Karakoram. *Geomorphology* **103**: 251–267. DOI:  
45 955 10.1016/j.geomorph.2008.04.026.  
46  
47  
48 956 Shennan I, Innes JB, Long AJ, Zong Y. 1995. Late Devensian and Holocene relative  
49 957 sea-level changes in northwest Scotland: new data to test existing models.  
50 958 *Quaternary International* **26**: 97–123.  
51  
52  
53  
54  
55  
56  
57  
58  
59  
60

- 1  
2  
3 959 Shroder JF, Owen LA, Seong YB, Bishop MP, Bush A, Caffee MW, Copland L, Finkel  
4 960 RC, Kamp U. 2011. The role of mass movements on landscape evolution in the  
5 961 central Karakoram: discussion and speculation. *Quaternary International* **236**: 34–  
6 962 47. DOI: 10.1016/j.quaint.2010.05.024.
- 7  
8  
9  
10 963 Sissons JB, Cornish R. 1982a. Rapid localised glacio-isostatic uplift at Glen Roy,  
11 964 Scotland. *Nature* **297**: 213–215.
- 12  
13  
14 965 Sissons JB, Cornish R. 1982b. Differential glacio-isostatic uplift of crustal blocks at  
15 966 Glen Roy, Scotland. *Quaternary Research* **18**: 268–288.
- 16  
17  
18 967 Smith DE, Stewart IS, Harrison S., Firth CR. 2009. Late Quaternary neotectonics and  
19 968 mass movement in South East Raasay, Inner Hebrides, Scotland. *Proceedings of*  
20 969 *the Geologists' Association* **120**: 145–154. DOI: 10.1016/j.pgeola.2009.08.006.
- 21  
22  
23 970 Soldati M, Corsini A, Pasuto A. 2004. Landslides and climate change in the Italian  
24 971 Dolomites since the Late glacial. *Catena* **55**: 141–161. DOI: 10.1016/S0341-  
25 972 8162(03)00113-9.
- 26  
27  
28 973 Stewart IS, Firth CR, Rust DJ, Collins PEF, Firth JA. 2001. Postglacial fault movement  
29 974 and palaeoseismicity in western Scotland: a reappraisal of the Kinloch Hourn fault,  
30 975 Kintail. *Journal of Seismology* **6**: 307–328.
- 31  
32  
33  
34 976 Stewart IS, Sauber J, Rose J. 2000. Glacio-seismotectonics: ice sheets, crustal  
35 977 deformation and seismicity. *Quaternary Science Reviews* **19**: 1367–1389.
- 36  
37  
38 978 Stock GM, Uhrhammer RA. 2010. Catastrophic rock avalanche 3600 years BP from El  
39 979 Capitan, Yosemite Valley, California. *Earth Surface Processes and Landforms* **35**:  
40 980 941–951. DOI:10.1002/esp.1982.
- 41  
42  
43 981 Stone JO. 2000. Air pressure and cosmogenic isotope production. *Journal of*  
44 982 *Geophysical Research* **105 (B10)**: 23753–23759.
- 45  
46  
47 983 Walker F. 1961. The Islay-Jura Dyke swarm. *Transactions of the Geological Society of*  
48 984 *Glasgow* **24**: 121–137.
- 49  
50  
51 985 Welkner D, Eberhardt E, Hermanns RL. 2010. Hazard investigation of the Portillo  
52 986 Rock Avalanche site, central Andes, Chile, using an integrated field mapping and  
53 987 numerical modelling approach. *Engineering Geology* **114**: 278–297. DOI:  
54 988 10.1016/j.enggeo.2010.05.007.
- 55  
56  
57  
58 989 Wilson P. 2004. Relict rock glaciers, slope failure deposits or polygenetic landforms?  
59  
60

- 1  
2  
3 990 A reassessment of some Donegal debris landforms. *Irish Geography* **37**: 77–87.  
4  
5 991 Xu S, Dougans AB, Freeman SPHT, Schnabel C, Wilcken KM. 2010. Improved Be-10  
6 and Al-26 AMS with a 5 MV spectrometer. *Nuclear Instruments and Methods* **B268**:  
7 992 736–738. DOI: 10.1016/j.nimb.2009.10.018.  
8 993  
9  
10  
11  
12  
13  
14  
15  
16  
17  
18  
19  
20  
21  
22  
23  
24  
25  
26  
27  
28  
29  
30  
31  
32  
33  
34  
35  
36  
37  
38  
39  
40  
41  
42  
43  
44  
45  
46  
47  
48  
49  
50  
51  
52  
53  
54  
55  
56  
57  
58  
59  
60

For Peer Review

1  
2  
3 *994* **Captions to Figures**

4  
5 *995*  
6 *996* **Figure 1.** The Paps of Jura, showing locations of RSF runout deposits and boulders  
7 *997* sampled for  $^{10}\text{Be}$  surface exposure dating. BOE: Beinn an Oir East RSF. BS: Beinn  
8 *998* Shiantaidh RSF. BCW: Beinn a'Chaolais West RSF. BCE: Beinn a'Chaolais East  
9 *999* RSF. BCS: Beinn a'Chaolais South RSF.

10 *1000*  
11 *1001* **Figure 2.** Sampled rock-slope failures. (a) Beinn Shiantaidh RSF; the failure scar is  
12 *1002* at the crest of the slope. (b) Beinn Shiantaidh RSF, showing the conspicuous arcuate  
13 *1003* outer ridge. (c) Beinn a'Chaolais South RSF runout lobe. The slope behind the runout  
14 *1004* lobe has apparently experienced deep-seated gravitational deformation. (d) Beinn  
15 *1005* a'Chaolais East RSF runout lobe. (e) Bouldery runout lobes of the Beinn a'Chaolais  
16 *1006* West RSF; samples were obtained from the lobe on the left. (f) Beinn an Oir East  
17 *1007* RSF.

18 *1008*  
19 *1009* **Figure 3.** Examples of sampled boulders. (a) Sample BS-06, Beinn Shiantaidh RSF.  
20 *1010* (b) Sample BCS-02, Beinn a'Chaolais South RSF. (3) Sample BCE-03, Beinn  
21 *1011* a'Chaolais East RSF. (4) Sample BOE-05, Beinn an Oir East RSF. Samples were  
22 *1012* obtained from the top surfaces of boulders. The hammer is 30 cm long.

23 *1013*  
24 *1014* **Figure 4.** The Sgriob na Caillich medial moraine. (a) Looking ESE towards Beinn an  
25 *1015* Oir. The arrow points to the failure scar of the RSF that appears to have provided the  
26 *1016* source of the debris on the moraine. (b) Looking WNW, and showing the bouldery, low  
27 *1017* relief nature of the moraine.

28 *1018*  
29 *1019* **Figure 5.** Exposure ages obtained for the five RSFs on Jura (vertical dashes). Top:  
30 *1020* ages calibrated using LL LPR. Bottom: ages calibrated using NWH11.6 LPR. Bars  
31 *1021* represent  $\pm 1\sigma$  total uncertainty. The vertical line represents the weighted mean  
32 *1022* deglaciation age and the shaded area represents the associated  $\pm 1\sigma$  uncertainty.  
33 *1023* Asterisk (\*) samples are anomalous outliers that significantly pre-date deglaciation  
34 *1024* or differ significantly from two other ages obtained from the same site.

35 *1025*  
36 *1026* **Figure 6** Top: Probability density distributions (PDDs) of the exposure ages  
37 *1027* obtained for the Scriob na Caillich moraine and the five RSFs on Jura, excluding  
38 *1028* outliers in both cases. Bottom: PDDs of the time elapsed since deglaciation based on  
39 *1029* PDDs shown on top. Left: ages calibrated using LL LPR. Right: ages calibrated using

1  
2  
3 1030 NWH11.6 LPR. The darker shaded zone represents  $\pm 1\sigma$  and the lighter shaded zone  
4 1031 represents  $\pm 2\sigma$ , demonstrating that all ages post-date the timing of deglaciation  
5  
6 1032 ( $t = 0$ ) at 95% confidence.  
7

8  
9 1033 .  
10 1034 **Figure 7.** Uncertainty-weighted mean ages for three Jura RSF runout deposit (BS,  
11 1035 BCS, BCE) and all postglacial ages for the remaining two (BCW, BOE) plotted  
12 1036 against: (1) crustal uplift rates for Arisaig (from Firth and Stewart, 2000); (2) the timing  
13 1037 of deglaciation of Jura (this study); (3) NGRIP ice core  $\delta^{18}\text{O}$  data for 7-18 ka  
14 1038 (Rasmussen *et al.*, 2006); (4) the ice core stages proposed by Lowe *et al.* (2008); and  
15 1039 (5) mean July temperature data inferred from chironomid assemblages in SE Scotland  
16 1040 (Brooks and Birks, 2000), matched to the NGRIP ice core data. Solid circles represent  
17 1041 ages calculated using LL LPR, and vertical dashes represent ages calculated using  
18 1042 NWH11.6 LPR. Solid horizontal lines represent  $\pm 1\sigma$  external uncertainties for the  
19 1043 weighted mean ages (BS, BCS, BCE) and the most probable individual ages for BCW  
20 1044 and BOE. Dashed horizontal lines represent  $\pm 1\sigma$  external uncertainties for the  
21 1045 younger ages obtained for BCW and BOE.  
22  
23  
24  
25  
26  
27  
28  
29  
30  
31  
32  
33  
34  
35  
36  
37  
38  
39  
40  
41  
42  
43  
44  
45  
46  
47  
48  
49  
50  
51  
52  
53  
54  
55  
56  
57  
58  
59  
60

**Table 1:** Sample locations and analytical details

Sample	AMS ID	Grid reference	Latitude (°N)	Longitude (°W)	Altitude (m)	Thickness (mm)	Density (g cm <sup>-3</sup> )	Shielding correction	<sup>10</sup> Be atoms g <sup>-1</sup> (quartz)
Sgriob na Caillich medial moraine									
SNC-02	b6534	NR 488 754	55.9063	06.0196	374	38	2.75	0.998	80594 ± 8846
SNC-03	b6535	NR 487 754	55.9062	06.0207	363	39	2.67	0.998	70486 ± 7288
SNC-06	b6637	NR 482 758	55.9093	06.0304	356	35	2.66	0.999	95643 ± 4334
SNC-07	b6638	NR 481 758	55.9092	06.0307	353	40	2.66	0.999	94685 ± 3698
Beinn Shiantaidh (BS) RSF									
BS-01	b5160	NR 521 748	55.9032	05.9659	383	15	2.65	0.984	88483 ± 3238
BS-03	b5163	NR 521 748	55.9034	05.9676	401	30	2.65	0.982	94096 ± 3428
BS-06	b5164	NR 521 747	55.9023	05.9652	382	27	2.70	0.989	86712 ± 3297
Beinn a'Chaolais West (BCW) RSF									
BCW-01	b5157	NR 482 734	55.8875	06.0273	400	24	2.64	0.973	70385 ± 2612
BCW-03	b5158	NR 482 734	55.8874	06.0269	410	29	2.65	0.972	58891 ± 2302
BCW-04	b5159	NR 482 733	55.8872	06.0269	408	24	2.71	0.972	89920 ± 3322
Beinn a'Chaolais South (BCS) RSF									
BCS-01	b5154	NR 489 727	55.8820	06.0163	402	36	2.69	0.977	83374 ± 2961
BCS-02	b5155	NR 489 727	55.8820	06.0163	400	33	2.65	0.977	90274 ± 3310
BCS-04	b5550	NR 489 728	55.8824	06.0164	418	26	2.65	0.977	83677 ± 3327
Beinn a'Chaolais East (BCE) RSF									
BCE-02	b5148	NR 493 731	55.8859	06.0102	440	52	2.67	0.974	56806 ± 2177
BCE-03	b5152	NR 493 731	55.8855	06.0100	428	33	2.65	0.982	83349 ± 3181
BCE-04	b5153	NR 493 730	55.8852	06.0101	421	40	2.67	0.977	79113 ± 2992
Beinn an Oir East (BOE) RSF									
BOE-03	b5554	NR 503 746	55.9001	05.9952	482	60	2.66	0.962	123328 ± 7195
BOE-04	b5555	NR 503 746	55.8999	05.9948	470	37	2.68	0.976	52963 ± 2084
BOE-05	b5556	NR 503 746	55.8999	05.9948	469	11	2.66	0.976	90402 ± 3610



**Table 2**  $^{10}\text{Be}$  exposure ages

Sample	LL LPR			NWH 11.6 LPR		
	Exposure age (ka)	Internal uncertainty (ka)	Total uncertainty (ka)	Exposure age (ka)	Internal uncertainty (ka)	Total uncertainty (ka)
<i>Scriob na Caillich moraine</i>						
SNC-02*	14.01	1.56	1.69	13.10	1.46	1.53
SNC-03*	12.35	1.30	1.41	11.55	1.21	1.28
SNC-06	16.88	0.78	1.10	15.78	0.73	0.92
SNC-07	16.82	0.67	1.03	15.73	0.63	0.84
Weighted mean	<b>16.84</b>	<b>0.51</b>	<b>0.93</b>	<b>15.75</b>	<b>0.47</b>	<b>0.53</b>
<i>Beinn Shiantaidh (BS) RSF</i>						
BS-01	15.18	0.56	0.90	14.19	0.53	0.73
BS-03*	19.22	0.71	1.14	17.97	0.67	0.92
BS-06	15.05	0.58	0.91	14.08	0.54	0.74
Weighted mean	<b>15.11</b>	<b>0.41</b>	<b>0.81</b>	<b>14.14</b>	<b>0.38</b>	<b>0.63</b>
<i>Beinn a'Chaolais South (BCS) RSF</i>						
BCS-01	14.39	0.52	0.84	13.45	0.49	0.68
BCS-02	15.58	0.58	0.92	14.56	0.54	0.75
BCS-04	14.10	0.57	0.86	13.19	0.53	0.71
Weighted mean	<b>14.66</b>	<b>0.32</b>	<b>0.75</b>	<b>13.70</b>	<b>0.30</b>	<b>0.57</b>
<i>Beinn a'Chaolais East (BCE) RSF</i>						
BCE-02*	9.56	0.37	0.57	8.94	0.35	0.47
BCE-03	13.92	0.54	0.84	13.02	0.50	0.68
BCE-04	13.44	0.52	0.81	12.57	0.48	0.65
Weighted mean	<b>13.67</b>	<b>0.37</b>	<b>0.73</b>	<b>12.78</b>	<b>0.35</b>	<b>0.57</b>
<i>Beinn a'Chaolais West (BCW) RSF</i>						
BCW-01	12.06	0.45	0.72	11.29	0.42	0.58
BCW-03	10.08	0.40	0.61	9.43	0.37	0.50
BCW-04	15.37	0.58	0.92	14.37	0.54	0.74
Weighted mean (not calculated)						
<i>Beinn an Oir East (BOE) RSF</i>						
BOE-03*	20.57	1.23	1.56	19.23	1.14	1.33
BOE-04	8.54	0.34	0.52	7.99	0.32	0.42
BOE-05	14.38	0.59	0.88	13.45	0.55	0.72
Weighted mean (not calculated)						

\* Outlier ages that predate deglaciation or differ at  $p < 0.05$  from two other consistent ages from the same site; these are excluded from calculation of the uncertainty-weighted mean ages. Scaling from CRONUS online calculator (Balco et al., 2008): wrapper script version 2.2; main calculator version 2.1; constants version 2.2.1; muons version 1.1. Internal uncertainties ( $\pm 1\sigma$ ) are analytical uncertainties on  $^{10}\text{Be}$  measurements only. Total uncertainties ( $\pm 1\sigma$ ) also incorporate uncertainties in calibration and scaling.

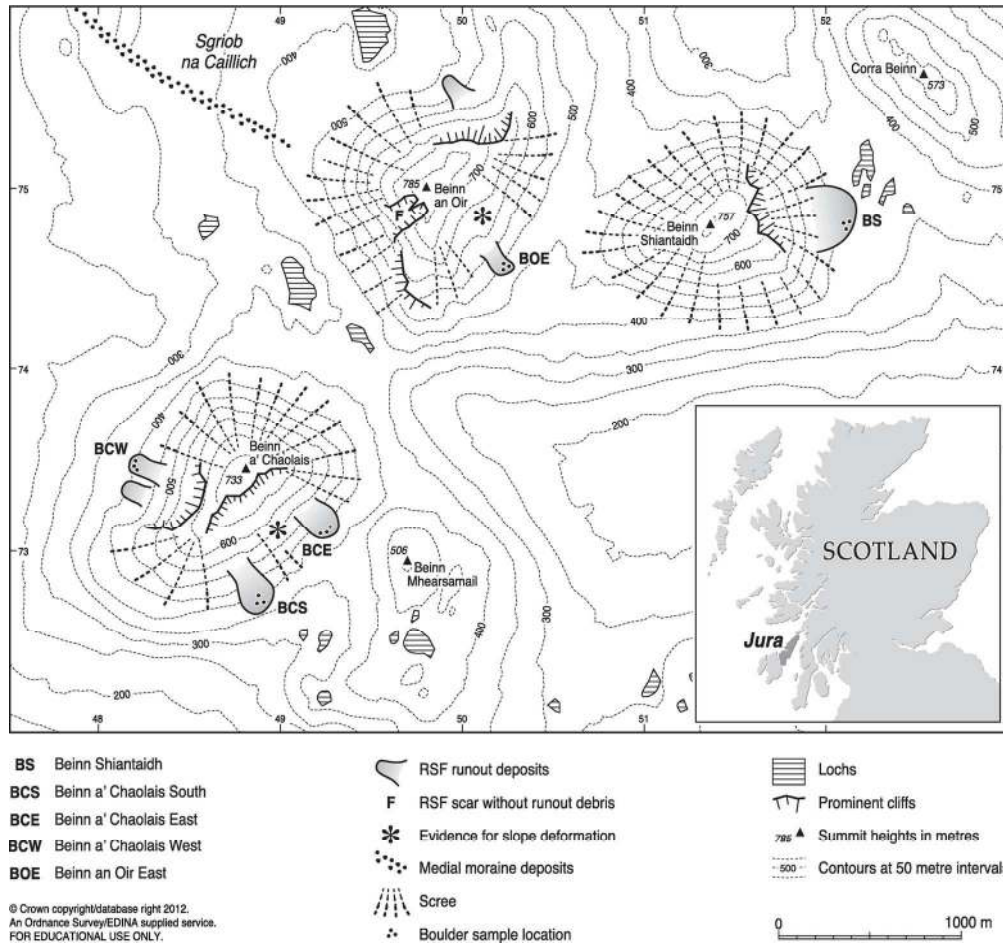


Figure 1. The Paps of Jura, showing locations of RSF runout deposits and boulders sampled for  $^{10}\text{Be}$  surface exposure dating. BOE: Beinn an Oir East RSF. BS: Beinn Shiantaidh RSF. BCW: Beinn a'Chaolais West RSF. BCE: Beinn a'Chaolais East RSF. BCS: Beinn a'Chaolais South RSF.  
146x137mm (300 x 300 DPI)



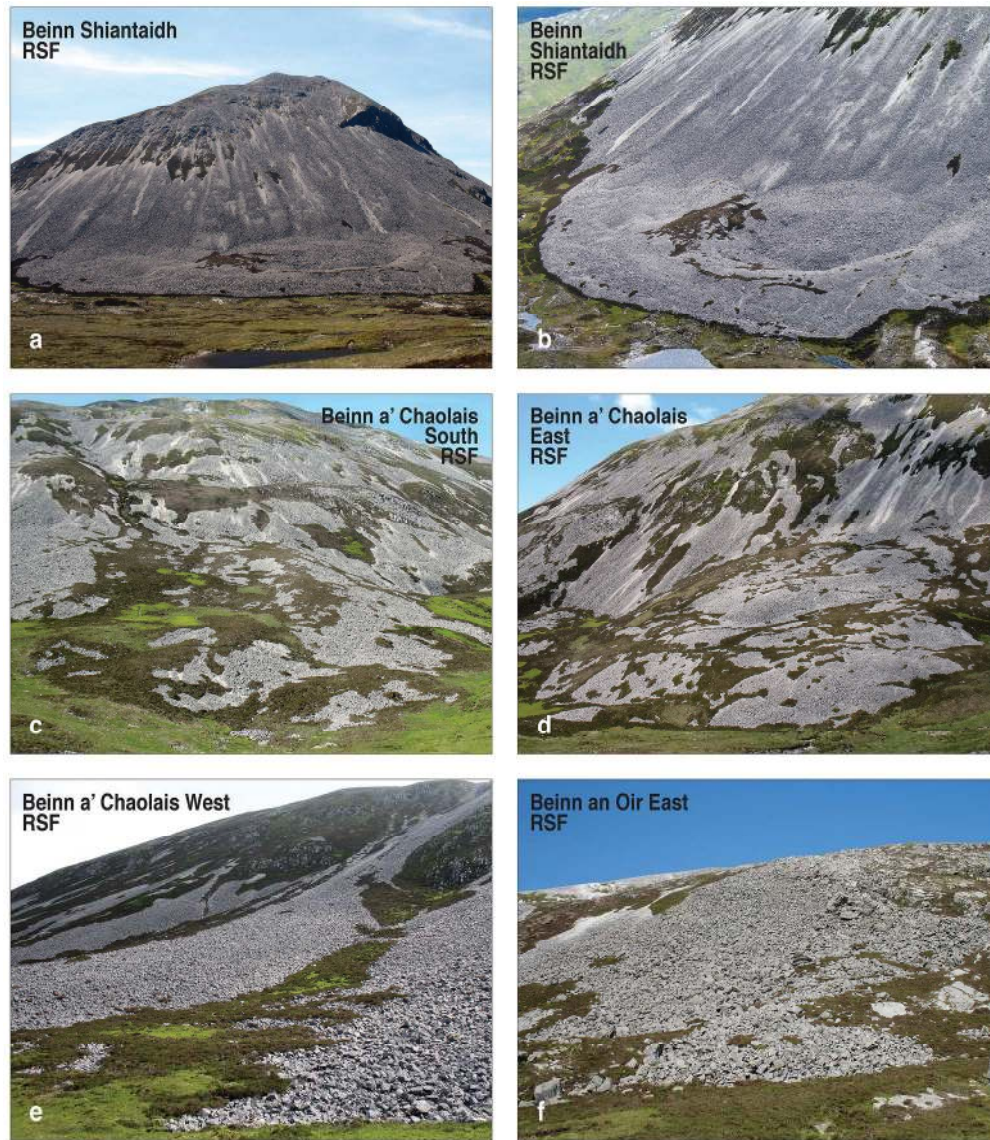


Figure 2. Sampled rock-slope failures. (a) Beinn Shiantaidh RSF; the failure scar is at the crest of the slope. (b) Beinn Shiantaidh RSF, showing the conspicuous arcuate outer ridge. (c) Beinn a'Chaolais South RSF runout lobe. The slope behind the runout lobe has apparently experienced deep-seated gravitational deformation. (d) Beinn a'Chaolais East RSF runout lobe. (e) Bouldery runout lobes of the Beinn a'Chaolais West RSF; samples were obtained from the lobe on the left. (f) Beinn an Oir East RSF.

181x207mm (300 x 300 DPI)



Figure 3. Examples of sampled boulders. (a) Sample BS-06, Beinn Shiantaidh RSF. (b) Sample BCS-02, Beinn a'Chaolais South RSF. (3) Sample BCE-03, Beinn a'Chaolais East RSF. (4) Sample BOE-05, Beinn an Oir East RSF. Samples were obtained from the top surfaces of boulders. The hammer is 30 cm long.  
120x92mm (300 x 300 DPI)



Figure 4. The Sgriob na Caillich medial moraine. (a) Looking ESE towards Beinn an Oir. The arrow points to the failure scar of the RSF that appears to have provided the source of the debris on the moraine. (b) Looking WNW, and showing the bouldery, low relief nature of the moraine.  
59x22mm (300 x 300 DPI)

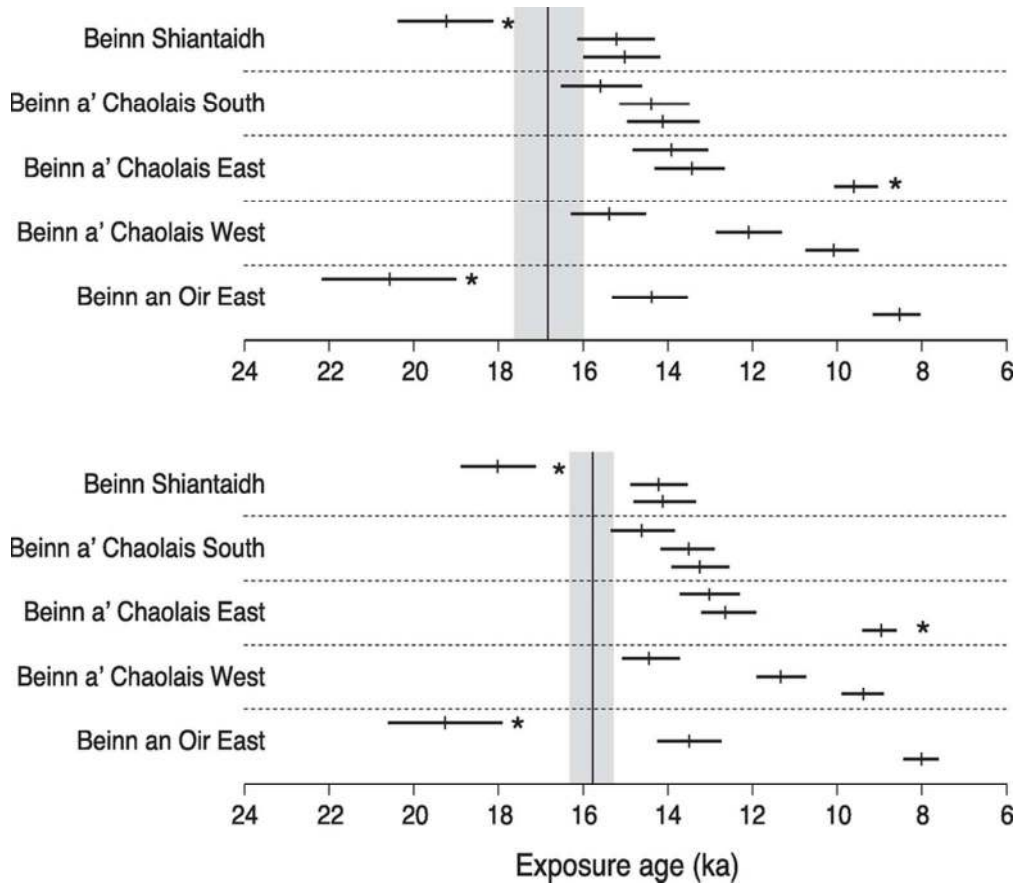


Figure 5. Exposure ages obtained for the five RSFs on Jura (vertical dashes). Top: ages calibrated using LL LPR. Bottom: ages calibrated using NWH11.6 LPR. Bars represent  $\pm 1\sigma$  total uncertainty. The vertical line represents the weighted mean deglaciation age and the shaded area represents the associated  $\pm 1\sigma$  uncertainty. Asterisk (\*) samples are anomalous outliers that significantly pre-date deglaciation or differ significantly from two other ages obtained from the same site.

81x70mm (300 x 300 DPI)



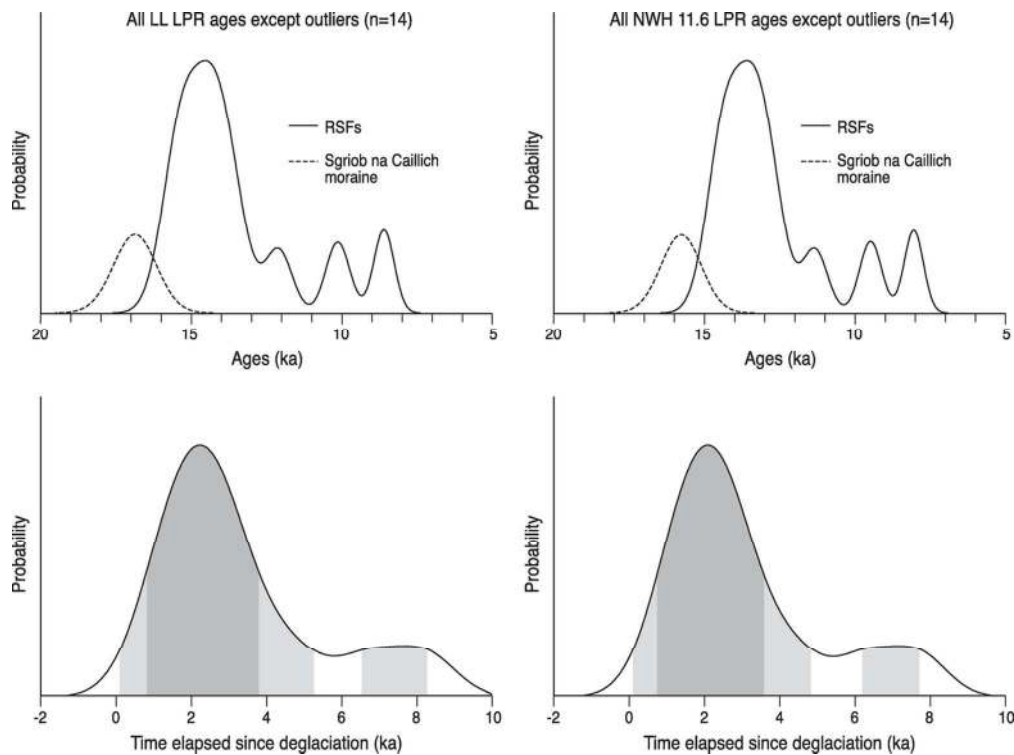


Figure 6 Top: Probability density distributions (PDDs) of the exposure ages obtained for the Sgriob na Caillich moraine and the five RSFs on Jura, excluding outliers in both cases. Bottom: PDDs of the time elapsed since deglaciation based on PDDs shown on top. Left: ages calibrated using LL LPR. Right: ages calibrated using NWH11.6 LPR. The darker shaded zone represents  $\pm 1\sigma$  and the lighter shaded zone represents  $\pm 2\sigma$ , demonstrating that all ages post-date the timing of deglaciation ( $t = 0$ ) at 95% confidence.

112x83mm (300 x 300 DPI)

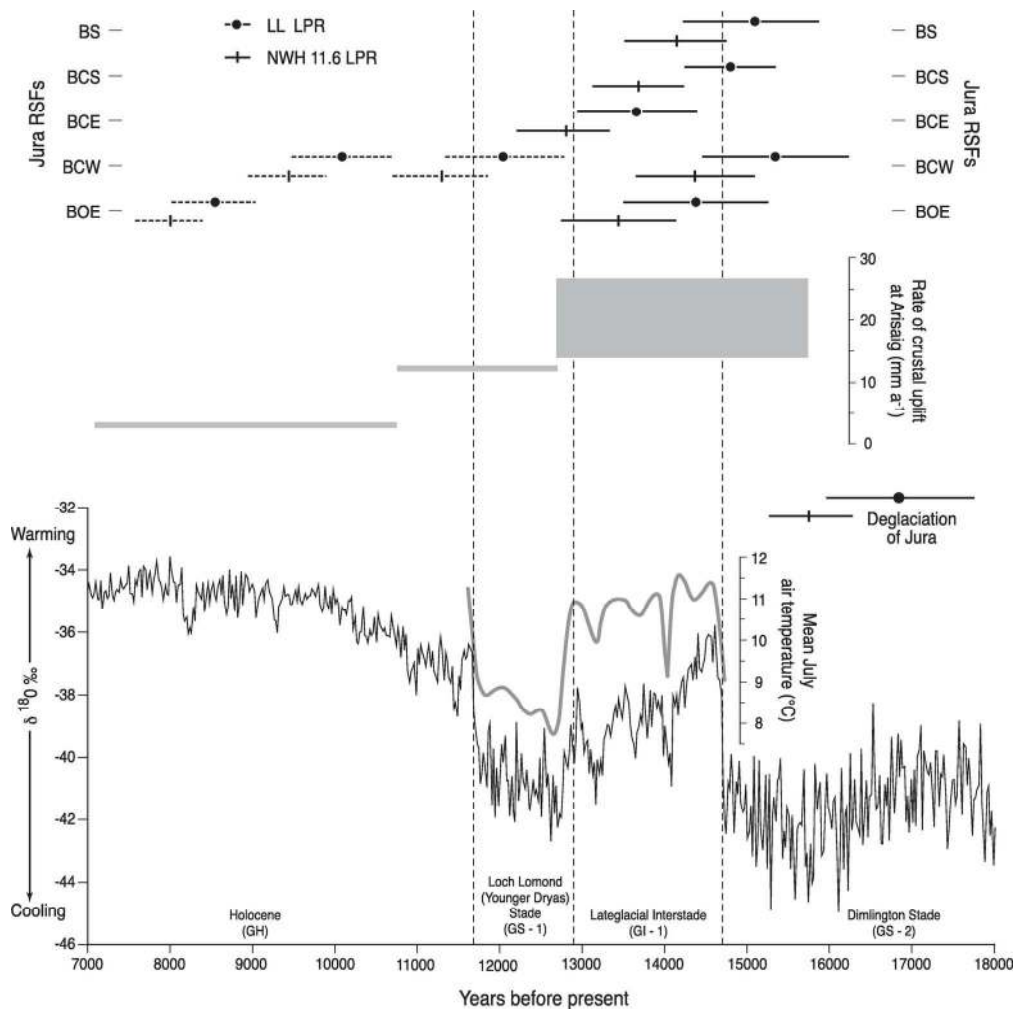


Figure 7. Uncertainty-weighted mean ages for three Jura RSF runout deposit (BS, BCS, BCE) and all postglacial ages for the remaining two (BCW, BOE) plotted against: (1) crustal uplift rates for Arisaig (from Firth and Stewart, 2000); (2) the timing of deglaciation of Jura (this study); (3) NGRIP ice core  $\delta^{18}\text{O}$  data for 7-18 ka (Rasmussen et al., 2006); (4) the ice core stages proposed by Lowe et al. (2008); and (5) mean July temperature data inferred from chironomid assemblages in SE Scotland (Brooks and Birks, 2000), matched to the NGRIP ice core data. Solid circles represent ages calculated using LL LPR, and vertical dashes represent ages calculated using NWH11.6 LPR. Solid horizontal lines represent  $\pm 1\sigma$  external uncertainties for the weighted mean ages (BS, BCS, BCE) and the most probable individual ages for BCW and BOE. Dashed horizontal lines represent  $\pm 1\sigma$  external uncertainties for the younger ages obtained for BCW and BOE.

155x155mm (300 x 300 DPI)